nature cancer

Article

https://doi.org/10.1038/s43018-026-01163-w

Adjuvant personalized multivalent neoantigen DNA vaccination for MGMT unmethylated glioblastoma: a phase 1 trial

Received: 19 August 2025

Accepted: 7 April 2026

Published online: 12 May 2026

Check for updates

A list of authors and their affiliations appears at the end of the paper

Glioblastoma is a fatal disease with a median prognosis of 12–18 months. Recent studies have shown encouraging results using neoantigen-based vaccines to stimulate glioblastoma-directed immune responses, but overall immunogenicity has been low. Here, we report the results of an open-label, single-arm, phase 1 clinical trial (GT-20) to evaluate the safety and feasibility (primary endpoints) as well as immunogenicity and preliminary clinical activity (secondary endpoints) of GNOS-PV01 monotherapy, a DNA-based personalized therapeutic cancer vaccine administered following surgical resection and radiation for patients with MGMT unmethylated glioblastoma. The GT-20 study vaccinated nine patients, using up to 40 neoantigens per patient (range, 17–40) without causing any serious adverse events, unexpected toxicities or dose-limiting toxicities. The vaccine induced activation and expansion of circulating peripheral T cells in all evaluated patients, except one who was being treated with dexamethasone. The secondary endpoint was to evaluate 6 month progression-free survival and 12 month overall survival; each observed in 66.7% of patients. Median progression-free survival was 8.5 months, median overall survival was 16.3 months and survival at 24 months was 33%, including one long-term survivor still alive 4 years from the time of initial surgery. This study met the pre-specified endpoints and supports the use of GNOS-PV01 as a potentially impactful component of glioblastoma immunotherapy. ClinicalTrials.gov: NCT04015700.

Glioblastoma (GBM) is the most common primary central nervous system malignancy in adults. It has a median overall survival of less than 20 months with standard-of-care surgical resection, radiotherapy and temozolomide chemotherapy[1,2]. Patients with GBM with unmethylated promoter regions of the *MGMT* (O^6-methylguanine methyltransferase) gene do not benefit from temozolomide, a DNA-damaging chemotherapy, owing to the active DNA repair mechanisms facilitated by high MGMT expression[3]. Therefore, new therapeutic options are desperately needed for this subgroup of patients.

Immune-activating therapies, such as immune checkpoint inhibitors, have demonstrated efficacy across many cancer types but have not improved survival in GBM. Randomized phase 3 studies showed no survival benefit from the addition of PD-1 blockade therapy to standard-of-care treatment in newly diagnosed patients[4,5] or at recurrence[6]. These poor responses may be attributed to extensive intra-tumoral heterogeneity, large populations of immunosuppressive myeloid cells, relatively low tumor mutational burden (TMB) and/or both local and systemic immune effector cell dysfunction[7,8]. Patients with GBM display profound T cell dysfunction owing to tumor-specific features[9] and to treatment with temozolomide and dexamethasone.

Neoantigen cancer vaccination is a versatile platform that has emerged as an approach to clonally expand and, potentially, repolarize

e-mail: tannerjohanns@wustl.edu

immune effectors that destroy malignant cells. In GBM, prior vaccination studies demonstrated that synthetic peptide vaccines generated T cell immunity to both patient tumor-specific neoantigens and to shared tumor-associated antigens[10–15]. In addition, cell-based approaches using infusion of autologous dendritic cells or mRNA pulsed with tumor lysate have shown similar results[16,17]. These initial studies have supported the feasible use and preliminary efficacy of therapeutic cancer vaccines in GBM, but further optimization of these platforms is needed, as cautioned by the failed randomized controlled trials to date[13,16]. As such, imparting durable anti-tumoral immunity will probably require a multi-epitope vaccine delivery system designed to target widely distributed antigens, with respect to the documented spatial heterogeneity of neoantigen diversity in GBM[18]. Incorporation of multi-sector sampling from multiple tumor sites served as a basis for neoantigen selection in the 'NeoVax' phase 1 clinical trial (ClinicalTrials.gov: NCT03422094), which identified a wider breadth of spatially heterogeneous candidate neoantigens in GBM[12]. However, the incorporation and subsequent evaluation of all candidates was constrained by manufacturing challenges related to cost, scalability, solubility and production time of the synthetic long peptide platform[12].

To address these challenges, we incorporated multi-sector sampling into the design and production of personalized neoantigen DNA vaccines, a platform that can accommodate a broader range of neoantigens than peptide vaccines[19]. Here, we report the results from nine patients enrolled in the 'GT-20' DNA vaccine phase 1 clinical trial (ClinicalTrials.gov: NCT04015700). For each patient, a bespoke DNA vaccine was generated, targeting up to 40 spatially distributed neoantigens (range, 17–40) using the same antigen selection strategy and personalized variant antigens by cancer sequencing (pVAC-seq) pipeline as previously described[12]. Vaccine-induced immune responses were evaluated through bulk T cell receptor (TCR) sequencing, in vitro functional assays and a unique method of T cell enrichment coupled with single-nuclei RNA sequencing (snRNA-seq). The results from this study will inform subsequent trials that aim to explore combinatorial therapeutic approaches in this disease setting to maximize efficacy.

Results

GT-20 trial overview

This phase 1 clinical trial aimed to assess the safety, feasibility and immunogenicity of a personalized neoantigen DNA vaccine platform (GNOS-PV01) in adult patients with newly diagnosed MGMT unmethylated GBM following surgical resection and radiotherapy (no temozolomide chemotherapy). In total, 34 patients were screened, of which 13 patients were deemed eligible; nine patients agreed to participation (Fig. 1a). The median age of the participants was 59 years (range, 54–68 years); 67% were male and 100% were white. Patient treatment history is summarized in Table 1. Three to four geographically distributed tumor regions were collected at the time of initial surgery to predict and select candidate neoantigens[12]. All vaccinations were given intramuscularly, followed by electroporation in combination with INO-9012, a DNA plasmid encoding interleukin-12 (IL-12), as a molecular adjuvant. The protocol allowed for vaccinations to continue until progression, intolerance or vaccine supply exhaustion. Correlative studies, including immunocyte deconvolution of bulk RNA-seq data through CIBERSORTx[20], TCR sequencing (TCR-seq), interferon-γ (IFNγ) ELISpot assay and flow cytometric intracellular cytokine staining, were performed using tumor specimens and serial peripheral blood mononuclear cell (PBMC) samples taken both pre and post vaccination (Fig. 1b). In addition, three patients underwent repeat resection following concern for radiographic progression, which allowed using bulk and snRNA-seq to evaluate transcriptional changes in the post-vaccination tumor and immune microenvironment.

Multiregional neoantigen identification

Three spatially distinct tumor regions for each patient were collected at initial surgery, except for patient 2, from whom four regions were collected owing to the larger tumor size. Whole-exome sequencing (WES) was performed on DNA extracted from all tumor regions and on matched normal PBMC-derived DNA. RNA-seq was performed from RNA extracted from all tumor regions. GBMs typically have a low TMB, which was consistently observed in our cohort with a median pre-vaccination ($n = 9$) TMB of 2.6 mutations per megabase (Supplementary Table 1). The integration of multi-sector sampling increased the number of identified variants by an average of 45% across all nine patients (range, 17–73%) by comparing to the tumor region with the least number of variants (Fig. 1c); a finding consistent with our prior NeoVax synthetic long-peptide-based trial[12]. Computational neoantigen prediction analysis and prioritization using pVAC-seq[21] was performed on data from all sampled regions to identify neoantigen candidates as previously described[12] (Supplementary Tables 2 and 3). In brief, a half-maximal inhibitory concentration (IC_{50}) human leukocyte antigen (HLA) binding affinity score of <500 nM and an RNA transcript per kilobase million (TPM) of >1 were used to prioritize vaccine neoantigens. Given that DNA-based vaccine platforms can accommodate a relatively higher neoantigen payload[22,23], the maximum number per patient for this study was capped at 40, unlike prior peptide-based vaccine studies, which limited the number of neoantigen candidates to 20 (refs. 10–12). A median of 36 (range, 17–40) neoantigens were included in each vaccine (Fig. 1d and Supplementary Table 4), and, importantly, the increased neoantigen payload capacity of the DNA platform enabled the inclusion of 100% of the candidate neoantigens in the vaccine for seven out of the nine (78%) enrolled patients. On average, 94.5% of neoantigens were derived from non-synonymous mutations; 3% derived from deletions, 1.5% from insertions and 1% from splice variants. There were no recurring neoantigens targeted across patients.

Consistent with a previously published report[18] and our prior peptide vaccine study[12], most variants were shared among all sampled regions (clonal); however, a notable number of variants (21–58%) were restricted to one or more regions (subclonal private or subclonal shared, respectively) (Fig. 1e). The spatial distribution of the final selected neoantigens for each patient's vaccine are shown in the respective donut plots (Fig. 1e). As expected, clonal and subclonal shared variants had the highest variant allele frequencies (Extended Data Fig. 1) and constituted the majority of prioritized neoantigen candidates, although subclonal private neoantigens were also included to encompass all aspects of tumor heterogeneity.

GNOS-PV01 is safe and well-tolerated

The personalized cancer vaccine for each patient was manufactured during the 6 weeks of standard radiation therapy. Following completion of radiation, patients received priming doses of vaccination (every

Fig. 1 | GT-20 trial overview. a, Consort diagram. **b**, Schematic sample characterization. **c**, Bar graph displaying the number of validated variants for each patient. Dark green bars show number of variants in the sampled region with the lowest number of variants; light green bars show number of unique variants among all sampled regions. **d**, Selection criteria for neoantigens included in the personalized vaccines. The mean or median of all nine patients is shown. **e**, UpSet plots displaying multi-sector sampling variant distribution for each patient. Subclonal private variants are restricted to one sampled region. Subclonal shared variants are found in more than one region but not all sampled regions. Clonal variants are shared among all sampled regions. Donut plots show the regional distribution of neoantigens included in each patient's vaccine. ICS, intracellular staining; IGV, integrated genomics viewer; IVS, in vitro stimulation; KPS, Karnofsky Performance Scale. Illustrations created in BioRender: **a**, Garfinkle, E. https://biorender.com/i65yunp (2026); **b**, Garfinkle, E. https://biorender.com/y7akihk (2026); **d**, Garfinkle, E. https://biorender.com/zt5p5rr (2026).

https://doi.org/10.1038/s43018-026-01163-w

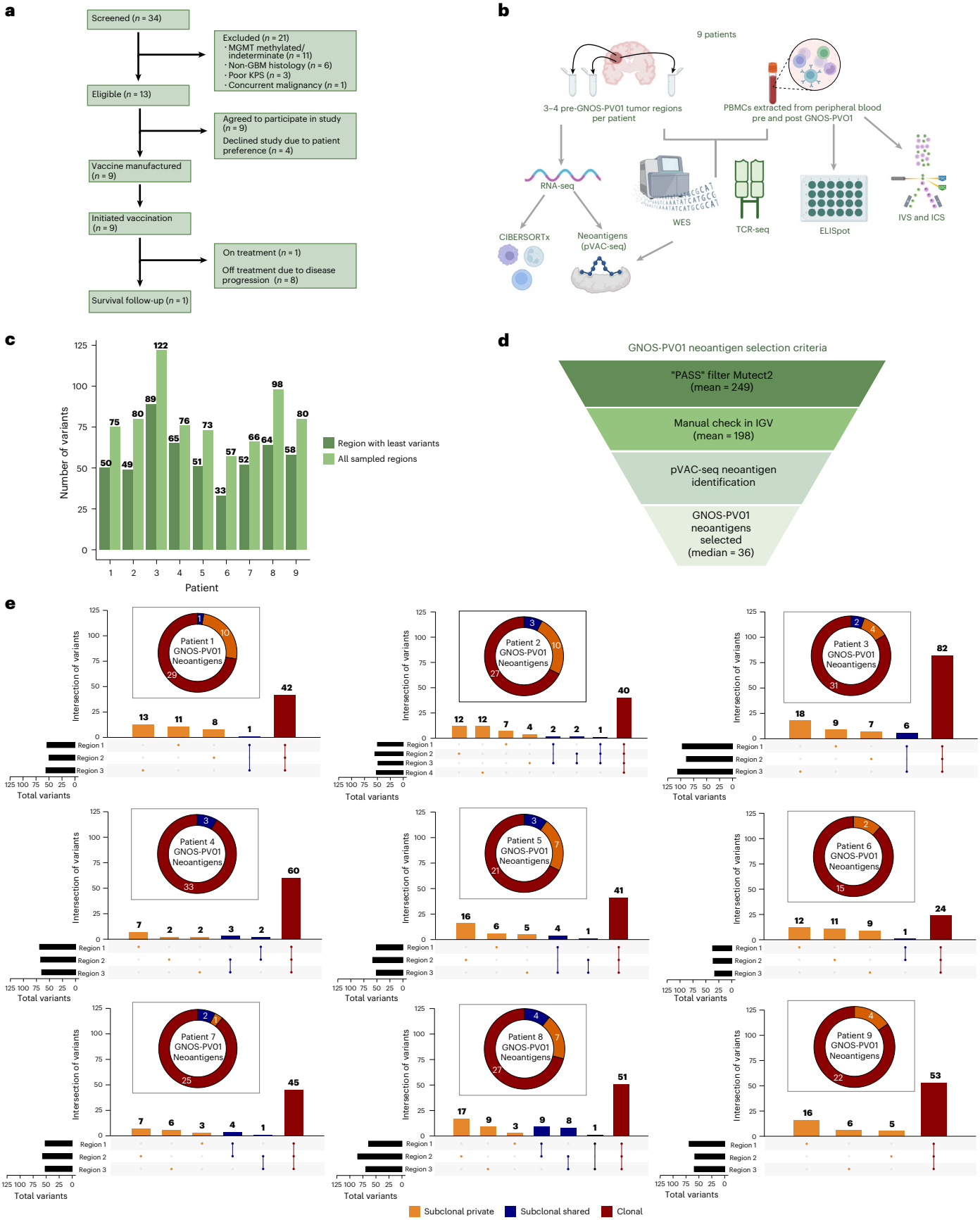

https://doi.org/10.1038/s43018-026-01163-w

Table 1 | GT-20 cohort overview

Patient	Volumetrics (cm^3) before surgery	Volumetrics (cm^3) after surgery	KPS	Dexamethasone (on C1D1 GNOS-PV01)	Tumor-treating fields	Bevacizumab for symptomatic edema	Treatment after GNOS-PV01 progression
1	NE: 155.88 E: 27.63	NE: 26.54 E: 0.99	70%	No	Yes	Pre-GNOS-PV01	Hospice
2	NE: 79.93 E: 46.71	NE: 54.00 E: 1.86	80%	Yes	Yes	Post-GNOS-PV01	Surgery Pembrolizumab Radiation Temozolomide
3	NE: 86.17 E: 23.69	NE: 21.52 E: 9.16	90%	No	No	Pre-GNOS-PV01	Hospice
4	NE: 201.52 E: 18.41	NE: 171.02 E: 5.16	90%	No	No	Pre-GNOS-PV01	Hospice
5	NE: 93.79 E: 67.32	NE: 47.00 E: 1.11	100%	No	No	Post-GNOS-PV01	Regorafenib Pembrolizumab;
6	NE: 101.45 E 28.7	NE: 16.47 E: 0.79	100%	No	No	No	Bevacizumab
7	NE: 35.78 E: 20.52	NE: 30.81 E: 0.79	100%	No	Yes	Post-GNOS-PV01	Hospice
8	NE: 68.72 E: 54.74	NE: 37.72 E: 0.61	100%	No	No	No	–
9	NE: 67.9 E: 0.778	NE: 30.91 E: 0.50	100%	No	No	No	Surgery Pembrolizumab Bevacizumab

Volumetrics were measured using Sectra IDS7 on available pre-operative and first available post-operative MRIs. E, enhancing post-contrast T1; NE, non-enhancing T2 FLAIR.

3 weeks for 9 weeks) followed by booster doses (every 9 weeks) (Fig. 2a). The primary endpoint of the study was to determine the safety and feasibility of GNOS-PV01. All nine participants in the study received the vaccine and were eligible for safety and feasibility assessments. Vaccine administration continued until progression, and no patient stopped vaccination owing to intolerance. A median of four doses was given to each patient (range, 2–18). There were no unexpected toxicities or dose-limiting toxicities reported in the study cohort. Most of the reported adverse events were grade 1 and related to injection site reaction (Table 2), which is consistent with prior DNA vaccine studies. No serious adverse events (per CTCAE v.4.0 grade 3 or greater) related to GNOS-PV01 were observed. After the dose-limiting toxicities period had lapsed, one patient experienced grade 3 cerebral edema (Table 2), noted as a slight worsening of baseline expressive aphasia and right upper extremity paresthesia. The patient was treated with low-dose bevacizumab (as per protocol guidelines), which led to a complete resolution of the symptoms and continuation of vaccination. In conclusion, the incorporation of more than 20 neoantigens did not alter the vaccine safety profile.

The feasibility endpoint was defined as the ability to manufacture and administer the personalized neoantigen DNA vaccine within 4 weeks of completion of radiotherapy; a time when standard-of-care adjuvant chemotherapy would otherwise be initiated. The median feasibility time (completion of radiotherapy to first vaccine administration) was 10 weeks (range, 5–18 weeks) and the median turnaround time (surgery to first vaccine administration) was 22 weeks (range, 17–30 weeks) (Supplementary Table 5). These results suggest that further pipeline optimization will need to be addressed for future trials to improve feasibility.

Outcome endpoints following vaccination

All nine patients enrolled in the study were included in the survival analysis. Of note, three of the patients (1, 2 and 9) had progressive disease after radiation but before receiving their first vaccine dose (Fig. 2b). The secondary endpoints of the study were 6 month progression-free survival and 12 month overall survival, which were both 66.7%. Additionally, the median progression-free survival and median overall survival from time of surgery for the entire GT-20 cohort were 8.5 months and 16.3 months, respectively (Fig. 2c). Moreover, the survival rate at 24 months was 33%, with one patient alive and disease-free more than 4 years from diagnosis (patient 8) (Fig. 2b). For reference, expected overall survival at 24 months would be 10–15% based on previous studies in the same patient population[3,4,24,25]. Furthermore, compared to a contemporaneous cohort of five patients with MGMT unmethylated GBM who received standard-of-care chemoradiotherapy instead of vaccine (four were eligible for GT-20 but declined because of personal preference and one had a history of a pre-existing malignancy that excluded trial eligibility but did not impact survival), the GT-20 cohort fared better. Indeed, the GT-20 cohort mirrored that of a contemporaneous cohort of seven patients with GBM who were ineligible for GT-20 solely owing to MGMT methylation status and received standard-of-care therapy (Extended Data Fig. 2). Given the limited sample size of these cohorts, survival differences did not reach statistical significance and limit broader comparative conclusions but serve as an institutional control.

Vaccination induces an activated peripheral T cell response correlated with improved survival

PBMCs were collected after radiotherapy but before vaccine initiation, and again after three priming doses of vaccine to assess immunogenicity. Owing to a lack of sufficient samples collected, patients 1 and 9 were not included in these assays. PBMCs were cultured ex vivo for 3 days with respective neoantigen peptides to enrich for antigen-specific T cells before restimulation (post hoc functional assay). There was a statistically significant increase in $CD8^+$ and $CD4^+$ T cells expressing activation markers (CD69, CD137 and PD-1) and the proliferation marker Ki67 following neoantigen stimulation compared to unstimulated controls (Fig. 3a). To assess the relationship between T cell activation and clinical outcomes, a Pearson's correlation test was performed between the percentage change (% delta) in CD69 and IFNγ expressed on $CD8^+$ and $CD4^+$ T cells and the overall survival from time of surgery. Interestingly, despite no significant difference observed in the expression of effector cytokines (CD107a, granzyme A, perforin, IFNγ) post vaccination (Extended Data Fig. 3), a significant positive correlation was observed between survival and percentage increase in $CD8^+CD69^+$ ($R = 0.84$, $P = 0.018$) and $CD8^+IFN\gamma^+$ ($R = 0.78$, $P = 0.04$)

https://doi.org/10.1038/s43018-026-01163-w

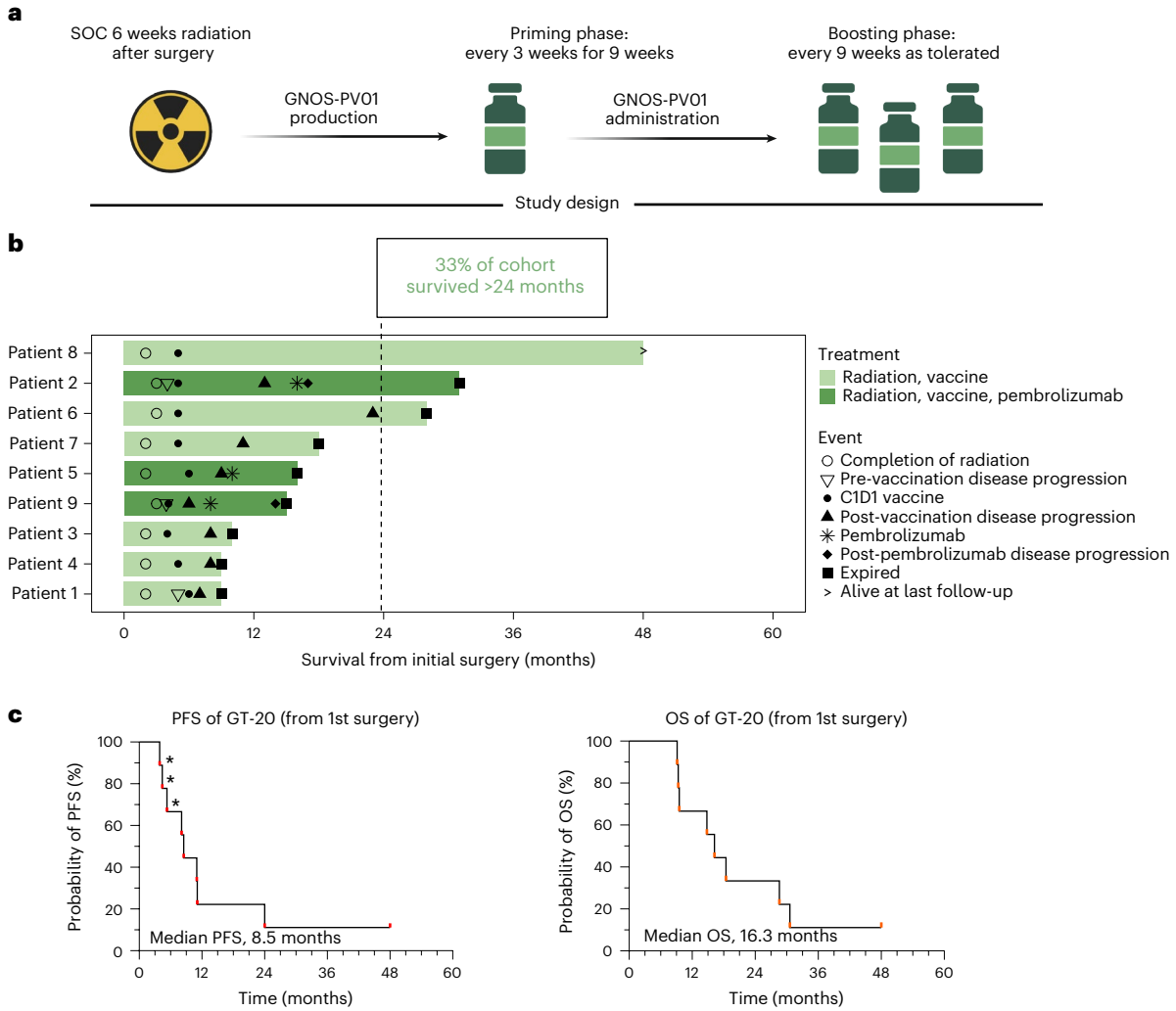

Fig. 2 | GT-20 trial outcomes. a, Schematic of study design. SOC, standard of care. Created in BioRender; Garfinkle, E. https://biorender.com/t5urg58 (2026). **b**, Swimmer plot displaying clinical outcomes from the time of initial surgery for all nine patients. **c**, Probability of progression-free survival (PFS; left) and overall survival (OS, right) from first surgery in all patients. Asterisk indicates patients who had progressive disease before receiving the vaccine. Significance was evaluated by the log-rank (Mantel–Cox) test.

T cells, whereas a similar correlation was not found for $CD4^+CD69^+$ ($R = -0.32$, $P = 0.48$) or $CD4^+IFN\gamma^+$ ($R = 0.21$, $P = 0.66$) T cells (Fig. 3b). To assess neoantigen-specific reactivity in peripheral blood T cells, we performed IFNγ ELISpot assays (pre-specified) for patients 2–8. PBMCs were cultured overnight with two separate peptide pools, each containing half the neoantigen load included in each patient's vaccine (Supplementary Table 6). Spot-forming units were counted and plotted as a stacked bar graph to quantify cumulative T cell reactivity. We observed a sustained increment in T cell reactivity against tumor neoantigens in six out of seven patients starting as early as the first on-treatment timepoint evaluated (cycle 2, day 8; C2D8, approximately 10 weeks from initiation of dosing) relative to levels at initiation of treatment (cycle 1, day 1; C1D1) (Fig. 3c). Importantly, the one patient (patient 2) who did not generate an augmented immune response post vaccination was receiving dexamethasone during vaccination, which has been shown to blunt reactivity[10]. In total, we found a statistically significant ($P = 0.0156$) increase in response after vaccination compared to baseline for the entire cohort (Fig. 3d). Notably, in patients with serial specimens available for analysis, we found the peak response occurred between cycles 3 and 6, or roughly 18 to 46 weeks after the initial vaccine dose (Fig. 3c). The continued expansion of neoantigen reactive T cell clones supports repeated vaccine dosing, and these data may have

Table 2 | GT-20 reported treatment-related adverse events

Treatment-related adverse events	Grade 1–2	Grade 3
Injection side reactions		
Pain, pain in extremity, musculoskeletal and connective tissue disorder–muscle soreness for 24 h after vaccine	7 (78%)	0
Gastrointestinal		
Nausea	2 (22%)	0
Nervous system		
Edema cerebral	0	1 (11%)
Dizziness	1 (11%)	0
Musculoskeletal		
Myalgia	1 (11%)	0
General		
Fatigue	1 (11%)	0
Psychiatric disorders		
Disoriented	1 (11%)	0

Treatment-related adverse events were reported in 7 out of 9 patients.

https://doi.org/10.1038/s43018-026-01163-w

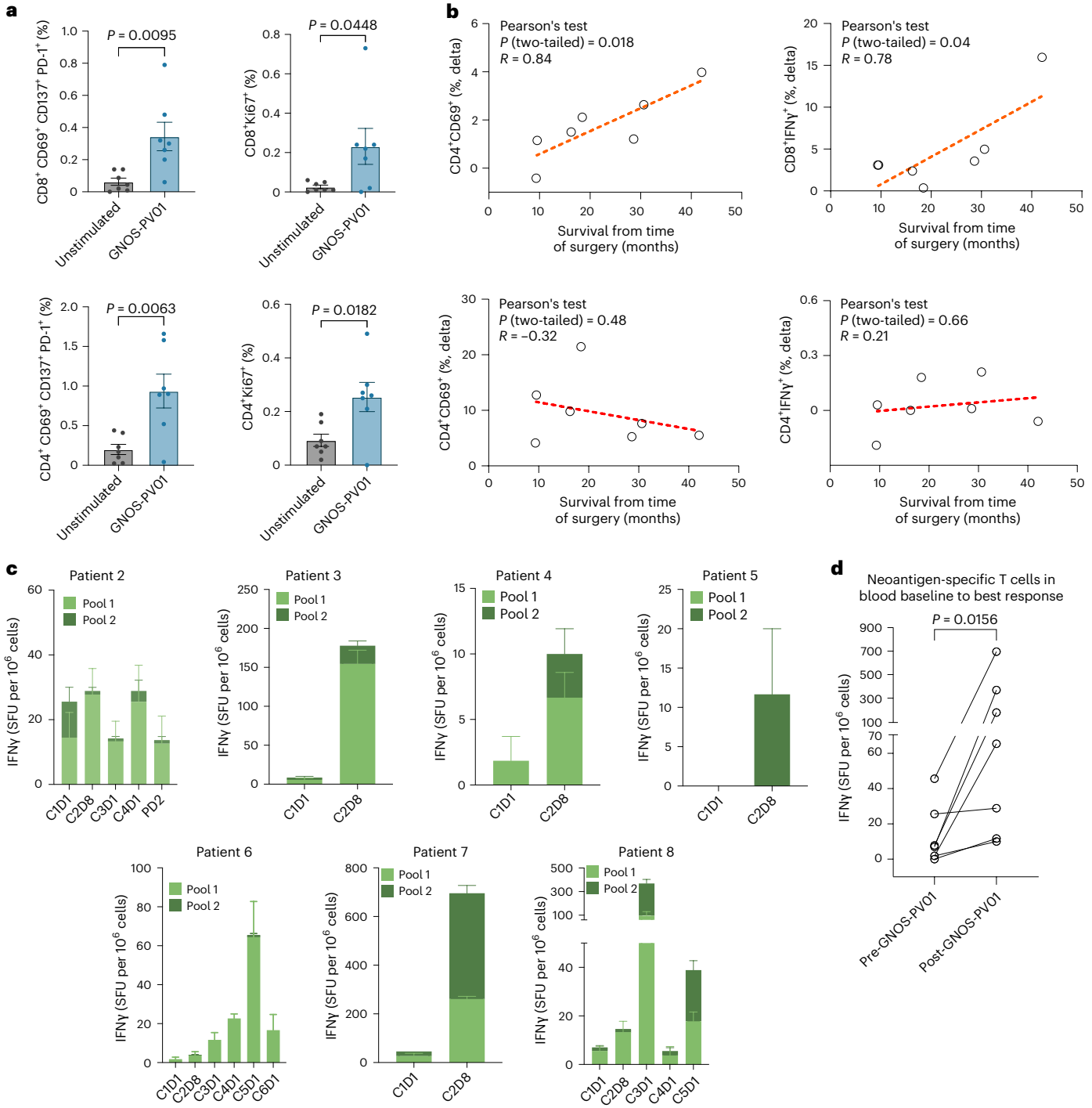

Fig. 3 | GNOS-PV01 drives polyfunctional T cell immunity. a, Individual $CD8^+$ or $CD4^+$ T cell markers from PBMCs were evaluated in seven patients (patients 2–8). A total of 2.5×10^5 post-GNOS-PV01 PBMCs from C2D8 for patients 2–7 and C2D1 for patient 8 were cultured in growth media with IL-2, IL-4 and IL-7 and enriched for neoantigen-specific T cells with 10 μg ml^{-1} of personalized neoantigen stimuli (GNOS-PV01) or controls (unstimulated). Cells were then stained intracellularly with surface markers for T cell activation (CD69, CD137 and PD-1) or proliferation (Ki67). Each filled circle represents a patient. Data are mean and s.e.m. *P* value was evaluated by two-tailed unpaired *t*-test with a Gaussian distribution. **b**, Two-tailed, Pearson's test correlation between percentage delta $CD69^+$ and $IFN\gamma^+$ for $CD8^+$ or $CD4^+$ T cells versus the overall survival from time of surgery (months) in seven patients (patients 2–8). **c**, T cell reactivity evaluated by IFNγ ELISpot upon two pool stimulations for individual patients, measured as spot-forming units (SFU) of $n = 3$ individual technical replicates per pool for all patients except patient 6. The stacked bars for patient 6 represent the mean SFU of two repeated ELISpot assays with three individual technical replicates for each assay. Data are mean and s.e.m. **d**, The magnitude of vaccine-induced responses evaluated by IFNγ ELISpot ($n = 7$). Stacked cumulative T cell reactivity was measured for patients 2–8. *P* value was evaluated by two-tailed Wilcoxon matched-pairs signed rank test.

underestimated the true immune reactivity of patients without serial PBMC sampling. These findings suggest that vaccine-driven activation of neoantigen-specific $CD8^+$ T cells contributes to an anti-tumor response associated with improved survival in this cohort.

Next, peptide deconvolution was performed to determine which individual neoantigen(s) induced reactivity. These analyses were limited to patients 6, 7 and 8 because they had sufficient PBMCs available. PBMC from baseline (before vaccination) and peak post-vaccination

timepoints were stimulated with individual vaccine-encoded peptides for 18–24 h. Cells were then evaluated for the presence of vaccine-induced neoantigen-specific responses by IFNγ ELISpot. We observed an increase in the number of unique neoantigens eliciting a response after vaccination in two out of the three patients (patients 7 and 8) (Extended Data Fig. 4a). The regional distribution of positive neoantigens after vaccination is reflective of the composition of each patient's vaccine, suggesting that vaccination was equally effective at inducing a T cell response against abundant clonal variants and subclonal variants (Extended Data Fig. 4b). We also observed a subset of neoantigens that stimulated reactivity both before and after vaccination, suggesting some post-vaccination responses are derived from pre-existing T cell memory rather than de novo induction.

Vaccination stimulates clonally expanded T cells in the GBM microenvironment

Patients 2 and 9 underwent repeat craniotomies for tumor resection of disease recurrence following vaccination. The resulting tissue permitted a unique opportunity to evaluate intra-tumoral responses to vaccination. Patient 2 had repeat resection 269 days after initial vaccination and before administration of pembrolizumab (Extended Data Fig. 5). Patient 9 had tumor resection 83 days after initial vaccination and before administration of pembrolizumab (Extended Data Fig. 6). Pembrolizumab was administered off-study at the discretion of the physician and through the manufacturer's expanded access program. WES and bulk RNA-seq were performed on the post-vaccination tumor resection samples. WES revealed that most of the variants in the post-vaccine tumor resections were shared with pre-vaccine tumor regions, although some new subclonal private and shared clonal mutations emerged (Fig. 4a and Extended Data Figs. 5c and 6c).

Bulk RNA-seq data were used to estimate immunocyte composition in the GBM microenvironment before and after vaccination using CIBERSORTx. Given that we selected neoantigens to include in the vaccine based on predicted ability to expand tumor-directed $CD8^+$ T cells, we focused on the imputed number of $CD8^+$ T cells from the CIBERSORTx analysis, revealing variability in the proportions of tumor-infiltrating T cells before and after vaccination. Patient 2 had relatively unchanged proportions of $CD8^+$ T cells across all pre-vaccination and post-vaccination tumor samples, consistent with a lack of increased T cell reactivity in the peripheral blood following vaccination (Fig. 4b). This result probably reflects the patient's ongoing steroid treatment throughout the post-operative and vaccination period. By contrast, Patient 9 had no to low $CD8^+$ T cell infiltration before vaccination but had a strong increase in $CD8^+$ T cell infiltration within the resection sample post vaccination, suggesting a vaccine-induced T cell response (Fig. 4b). To further validate these inferred changes in RNA-based imputation of $CD8^+$ T cell frequency, immunohistochemical assessment of representative pre-vaccine and post-vaccine tissues supported an insignificant increase in $CD8^+$ T cells for patient 2 ($P = 0.1391$, 53 cells per mm^2 versus 134 cells per mm^2) and a significant ($P = 0.0194$, 50 cells per mm^2 versus 181 cells per mm^2) increase for patient 9, confirming the CIBERSORTx results (Fig. 4c).

If vaccination administration successfully stimulates neoantigen-specific T cells, we would expect to see a clonal expansion of tumor-directed T cells in the peripheral blood and within the tumor. To assess changes in TCR repertoire diversity of patients 2 and 9 before and after vaccination, we performed post hoc bulk TCR-seq using ImmunoSEQ (Adaptive Biotechnologies) (Supplementary Table 7). We first identified the top 20 clones by frequency in the respective post-vaccination tumor resection samples for patients 2 and 9. After removing known viral-reactive T cell clones with TCRMatch[26] ($n = 2$ for each patient), the frequency of the remaining clones for each patient was plotted across pre-vaccination and post-vaccination tumor and available PBMC samples. Post-vaccination tumor-infiltrating clones were categorized as either new (not detected in a pre-vaccination tumor sample) or expanded (detected in at least one pre-vaccination tumor sample). Consistent with a lack of increased $CD8^+$ T cells in the tumor microenvironment after vaccination for patient 2 (Fig. 4b), we did not identify any clones exclusive to the post-vaccination tumor microenvironment (Fig. 4d). In patient 9, for whom we observed an increase in $CD8^+$ T cells after vaccination (Fig. 4b), six new clones exclusive to the post-vaccination resection were identified. Two of these (CASSPGTGFFYGYTF and CASSQDLDVLYEQYF) were also expanded in the peripheral blood after vaccination and further increased in frequency after administration of pembrolizumab (Fig. 4e). Unfortunately, sufficient PBMCs were not available for patient 9 to fully characterize the corresponding post-vaccine neoantigen-specific T cell reactivity. Regardless, these results suggest that response to vaccination can lead to both peripheral and intra-tumoral increases in T cell clonality.

Transcriptional landscape of the GBM tumor immune microenvironment

In-depth characterization of T cells from the GBM immune microenvironment by single-cell RNA-seq from fresh tissue has been successfully demonstrated[27]; however, processing of fresh tissue is not always feasible because of the timing of surgery or staff availability, or when samples need to be sent to other institutions for analysis. With whole cells from disrupted fresh tissue, rare T cell populations can be enriched using anti-CD3 antibody surface staining followed by flow-cytometry-based cell sorting, permitting a focused single-cell T cell analysis[27]. Single-cell sample preparation from frozen tissue involves isolating nuclei rather than whole cells from the bulk specimen, precluding the ability to further enrich T cells based on cell surface protein markers. Owing to the relative paucity of T cells within a GBM specimen, unenriched frozen tissue specimens limit the analysis of vaccine-induced T cell alterations. To overcome this technical challenge, we developed an innovative post hoc flow-cytometry-based method for enriching T cell nuclei from frozen specimens by staining for the T cell nuclear marker NFATc1 (Fig. 5a and Extended Data Fig. 7a). We performed snRNA-seq on frozen specimens from patients 2 (pre-vaccine region three and post-vaccine resection) and 9 (pre-vaccine region two and post-vaccine resection). Each sample was repeated in biological replicate, for a total of eight samples, and snRNA-seq data were annotated using the GBmap[28] (Fig. 5b,c and Extended Data Fig. 7b).

Subsetting on the enriched T cell nuclei, we identified three subtypes of $CD4^+$ T cells (central memory, activated and $GZMK^+$ exhausted)[27] and two subtypes of $CD8^+$ T cells ($GZMK^+$ activated and $GZMK^+$ exhausted) (Fig. 5d and Extended Data Fig. 7c). To investigate potential transcriptional differences in the post-vaccination setting between patients 2 and 9, who differed in dexamethasone usage and outcomes, we plotted expression of *CD69* and *PDCD1* (encoding PD-1) in the two $GZMK^+$ $CD8^+$ T cell subsets (Fig. 5e). We found a statistically significant increase in *CD69* expression in both activated ($P = 0.042$) and exhausted ($P = 2.6 \times 10^{-7}$) subsets for patient 9 compared to patient 2 but did not find a statistical difference in *PDCD1* expression. Unfortunately, even with T cell enrichment, we were unable to capture enough T cells from patient 9 before vaccination to perform differential expression and pathway analysis. Consequently, we only report results for $GZMK^+$ $CD8^+$ T cells from patient 2. Gene set enrichment analysis (GSEA) identified downregulation of immune system regulation, defense response, ATP metabolism and cellular response to stress pathways in the post-vaccination tumor resection (Extended Data Fig. 7d). This finding suggests that despite the relative consistency in the phenotype of infiltrating $GZMK^+$ $CD8^+$ T cells, these immunocytes are transcriptionally less responsive post vaccination, presumably owing to the immunosuppressive effects of dexamethasone. To further interrogate potential transcriptional changes that may affect T cell activation in patient 2, we performed GSEA on the dendritic cells and found downregulation of cellular response to stress, lymphocyte activation and immune response pathways in the post-vaccination tumor resection, suggesting

https://doi.org/10.1038/s43018-026-01163-w

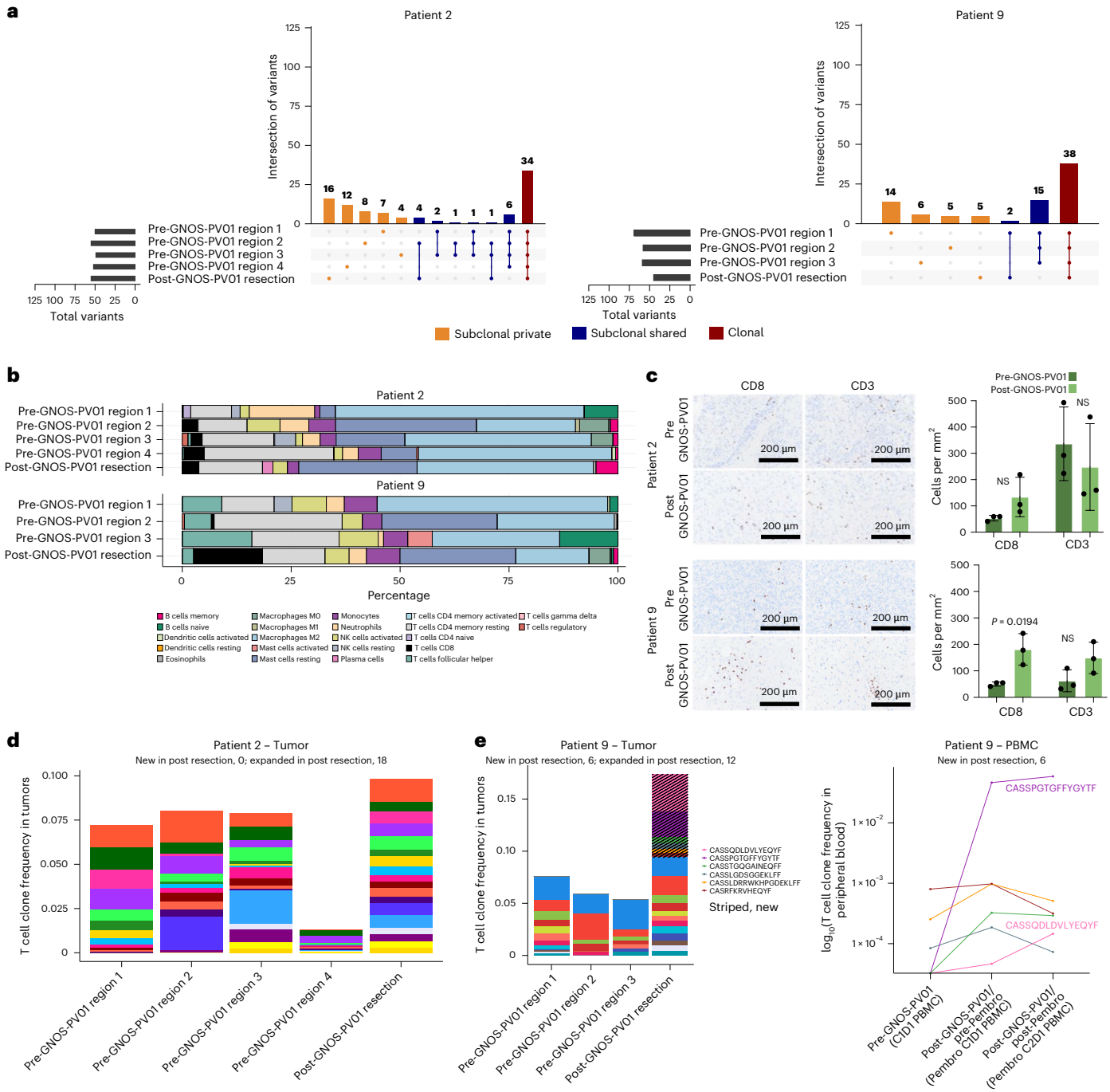

Fig. 4 | Post-GNOS-PV01 GBM microenvironment evaluation for patients 2 and 9. a, UpSet plots displaying multi-sector sampling variant distribution for each patient grouped by region with the inclusion of a post-GNOS-PV01 tumor resection. Subclonal private variants are restricted to one sampled region. Subclonal shared variants are found in more than one region but not all sampled regions. Clonal variants are shared among all sampled regions. **b**, Percentage of regional tumor-infiltrating immunocytes deconvoluted by the CIBERSORTx algorithm for each patient. The proportion of $CD8^+$ T cells is colored black. NK cells, natural killer cells. **c**, Representative immunohistological images for CD3 and CD8 pre-GNOS-PV01 and post-GNOS-PV01 for patients 2 and 9. Images were taken with a ×20 objective. Bar graph displays manually counted cells per mm^2 at three selected hotspot areas from a representative tumor block from either pre-GNOS-PV01 or post-GNOS-PV01 resection. Data are mean and s.d. *P* value evaluated by two-tailed, unpaired *t*-test. NS, not significant. **d**,**e**, Frequency of top 18 expanded T cell clones identified in patient 2 (**d**) and patient 9 (**e**) post-GNOS-PV01 tumor resection by bulk TCRβ sequencing. T cell clone frequency for all sampled pre-tumor and post-tumor samples is plotted. New clones are defined as present only in the post-vaccine tumor resection sample, and expanded clones are defined as present at a lower frequency in at least one pre-vaccine tumor sample compared to the post-vaccination sample. **e**, New clones are indicated by striped bars. Peripheral blood frequency of the six new clones identified in patient 9 post-GNOS-PV01 tumor resection at three timepoints is plotted (C1D1, before vaccination; Pembro C1D1, after vaccination but before pembrolizumab; C2D1, after vaccination and after one dose of pembrolizumab).

suppression in the post-vaccine tumor microenvironment, also probably a result of treatment with dexamethasone (Extended Data Fig. 7e).

To assess for potential tumor-intrinsic transcriptional changes that could be associated with responsiveness to GNOS-PV01 vaccination, we evaluated changes in neoplastic cell populations. The expression of HLA class I surface expression on tumors is essential for binding and presenting neoantigens to the immune system[29], and loss of *B2M*, a key component of HLA class I molecules, is associated with

https://doi.org/10.1038/s43018-026-01163-w

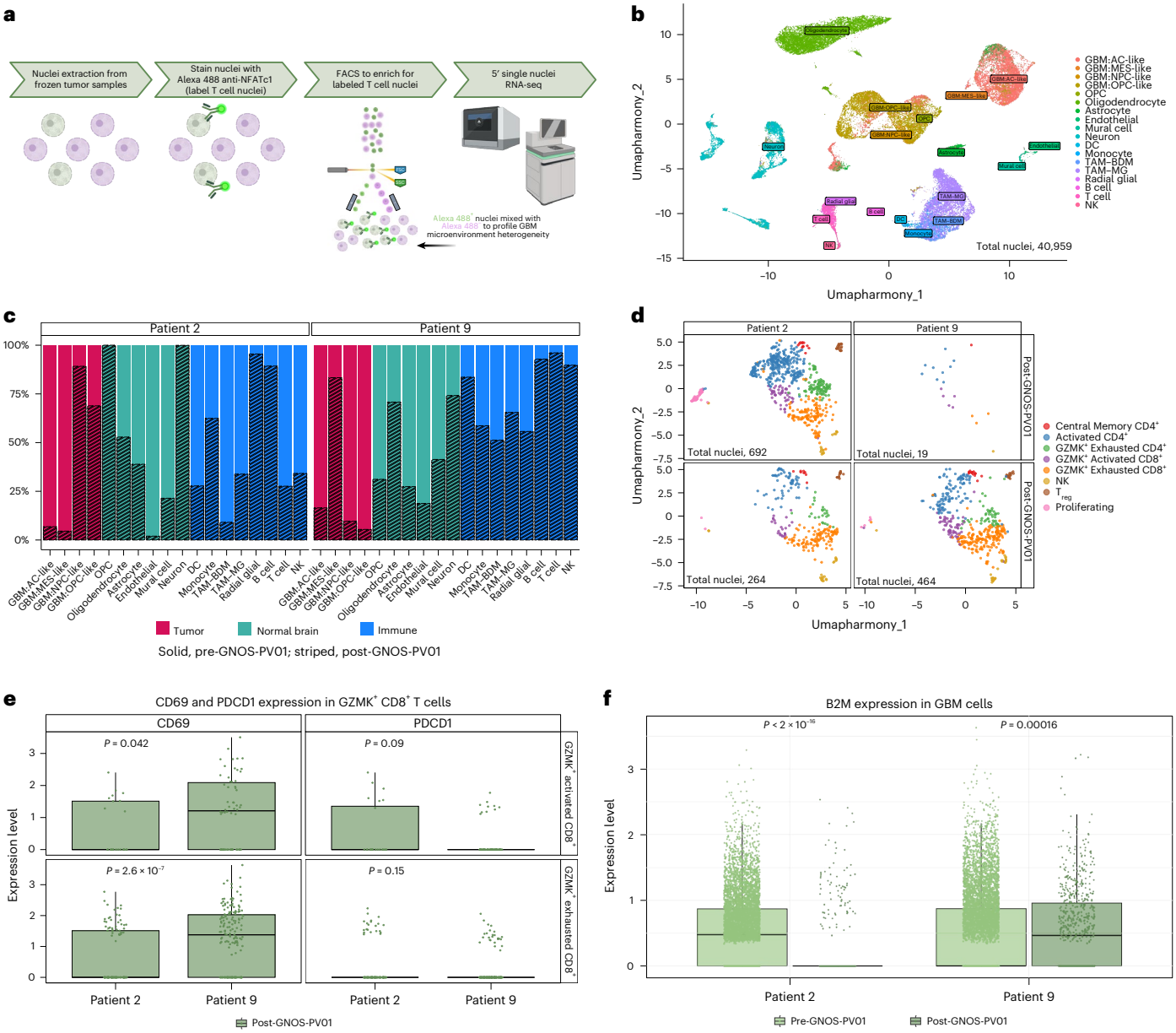

Fig. 5 | snRNA-seq defines transcriptional profiles of the GBM microenvironment before and after GNOS-PV01. a, Schematic of nuclei isolation from pre-GNOS-PV01 and post-GNOS-PV01 frozen tumor samples for patients 2 and 9, followed by staining for NFATc1 to enrich for T cells. Nuclei were then used as input for 5′ single-nuclei gene expression library preparation (10× Genomics) and sequencing (NovaSeq6000). Created in BioRender; Garfinkle, E. https://biorender.com/celopys (2026). **b**, Uniform manifold approximation and projection (UMAP) visualization of 40,959 total nuclei (eight total Harmony integrated samples; pre-GNOS-PV01 and post-GNOS-PV01 samples from patients 2 and 9 each prepared in biological replicate). Cell types were annotated using the GBmap reference. **c**, Bar graph showing percentage composition of each cell type grouped by category (tumor, normal brain or immune) and patient (2, 9) pre GNOS-PV01 (solid bar) and post GNOS-PV01 (striped bar). **d**, T cells from each sample were computationally subset and re-integrated using Harmony for subtyping based on key gene expression markers. UMAP visualization of 1,439 total T cells split by patient and timepoint is displayed. **e**, Expression of *CD69* and *PDCD1* for patients 2 and 9 post-GNOS-PV01 samples in GZMK$^+$ activated and exhausted CD8$^+$ T cells is displayed in boxplots. **f**, All GBM cells were computationally subset, and expression of *B2M* is shown in a violin plot across patients 2 and 9 pre GNOS-PV01 and post GNOS-PV01. For boxplots in **e** and **f**, boxes represent the interquartile range (IQR), center line designates the median, whiskers extend to 1.5× IQR and each dot represents a single cell. Statistical significance was calculated across timepoints using unpaired two-tailed Wilcoxon rank test. AC-like, astrocyte-like; DC, dendritic cell; MES-like, mesenchymal-like; NPC-like, neural progenitor cell-like; OPC-like, oligodendrocyte progenitor cell-like; OPC, oligodendrocyte progenitor cell; TAM-BDM, tumor-associated macrophage that originates from bone marrow; TAM-MG, tumor-associated macrophage that originates from microglia; T_{reg}, regulatory T cells.

acquired resistance to immunotherapy[30]. We computationally subsetted all the tumor cells and then plotted *B2M* expression across patients and between timepoints. Strikingly, patient 2 had a significant ($P < 2 \times 10^{-16}$) reduction in tumor cells expressing *B2M* after vaccination compared to patient 9, for whom *B2M* expression significantly ($P = 0.00016$) increased (Fig. 5f). To evaluate expression changes in neoantigen-relevant HLA alleles, we aligned our bulk RNA-seq data to an HLA class I reference. Consistent with the single-nuclei data, we found downregulation of each class I allele after vaccination in patient 2 (Extended Data Fig. 8a) compared with overall upregulation of four out of six alleles in patient 9 (Extended Data Fig. 8b). We did not find an association between expression of neoantigen-relevant alleles and neoantigen expression (Extended Data Fig. 8c,d), suggesting a more global HLA downregulation.

https://doi.org/10.1038/s43018-026-01163-w

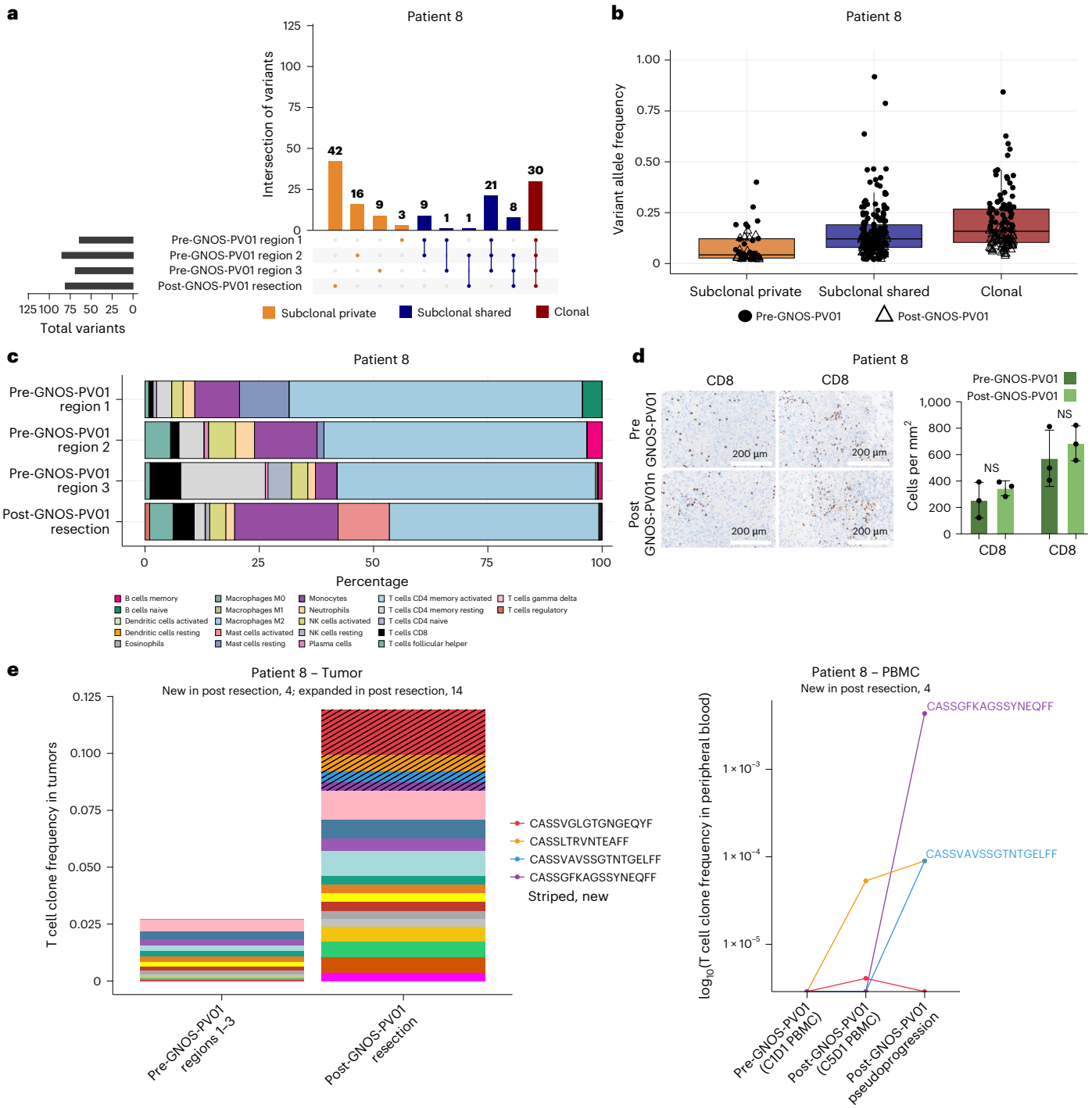

Fig. 6 | Tumor immune microenvironment characterization of a long-term survivor. a, UpSet plot displaying multi-sector sampling variant distribution for patient 8 grouped by region with the inclusion of a post-GNOS-PV01 tumor resection. Subclonal private variants are restricted to one sampled region. Subclonal shared variants are found in more than one region but not all sampled regions. Clonal variants are shared among all sampled regions. **b**, DNA variant allele frequency of variants grouped by regional distribution from pre-GNOS-PV01 and post-GNOS-PV01 tumor resection. Boxes represent the IQR, center line designates the median, whiskers extend to 1.5× IQR and each dot represents a variant. **c**, Percentage of regional tumor-infiltrating immunocytes deconvoluted by the CIBERSORTx algorithm. The proportion of $CD8^+$ T cells is colored black. **d**, Representative immunohistological images for CD3 and CD8 pre GNOS-PV01 and post GNOS-PV01. Images were taken with a ×20 objective. Bar graph displays manually counted cells per mm^2 at three selected hotspot areas from a representative tumor block from either pre-GNOS-PV01 or post-GNOS-PV01 resection. Data are mean and s.d. *P* value evaluated by two-tailed, unpaired *t*-test. **e**, Frequency of top 18 expanded T cell clones identified in patient 8 post-GNOS-PV01 tumor resection by bulk TCRβ sequencing. T cell clone frequency for all sampled pre-tumor and post-tumor samples is plotted. New clones are defined as present only in the post-vaccine tumor resection sample, and expanded clones are defined as present at a lower frequency in at least one pre-vaccine tumor sample compared to the post-vaccination sample. Peripheral blood frequency of the four new clones identified in patient 8 post-GNOS-PV01 tumor resection at three timepoints is plotted.

Long-term survivor demonstrates intra-tumoral T cell expansion and late peripheral T cell expansion

Patient 8 is currently recurrence-free more than 4 years from the time of diagnosis, but did develop transient magnetic resonance imaging (MRI) changes (first and second pseudoprogression lesions) followed by progressive changes concerning for disease recurrence (Extended Data Fig. 9). Although the two pseudoprogression lesions spontaneously resolved, the emergence of a progressive lesion led to the need for a diagnostic biopsy. The pathology report revealed treatment-related changes with areas of necrosis and no overt evidence of active disease. The patient did not receive any additional treatment after the biopsy and is still recurrence-free over 1 year post biopsy. As with patients 2 and 9, most of the tumor variants in the post-vaccine biopsy were shared with the pre-vaccine tumor regions, but there were also several post-vaccination subclonal private variants (Fig. 6a,b). CIBERSORTx analysis revealed consistent proportions of $CD8^+$ T cells across all pre-vaccination and post-vaccination tumor samples (Fig. 6c). Immunohistochemical assessment showed an increase in $CD8^+$ T cells (256 cells per mm^2 versus 345 cells per mm^2) but did not reach statistical significance (Fig. 6d). TCR-seq identified four clones exclusive to the post-vaccination tumor resection, two of which (CASSGFKAGSSYNEQFF and CASSVAVSSGTNTGELFF) were also expanded in the peripheral blood taken before biopsy (Fig. 6e). Taken together, these data highlight the impact of extended vaccination on the maintenance and evolving diversification of immune surveillance.

Discussion

We have shown that personalized neoantigen DNA vaccines, using the GNOS-PV01 platform, are safe and well-tolerated in the post-radiotherapy adjuvant setting. This platform permits the inclusion of up to 40 neoantigens without additional toxicity in patients with primary GBM. This result is consistent with findings from a recently published study (GT-30) in hepatocellular carcinoma, in which a similar multi-epitope DNA vaccine containing up to 40 neoantigens (GNOS-PV02) was combined with pembrolizumab, demonstrating safety as well as encouraging immunogenicity and efficacy data[19]. At the time our study was initiated, neoantigen vaccines had not targeted more than 20 neoantigens, and therefore an escalation to 40 neoantigen targets required a phase 1 study evaluating safety. Since that time, mRNA vaccine strategies incorporating up to 34 neoantigens have been evaluated in melanoma[31], further supporting the safety of higher neoantigen numbers and the promise of nucleic-acid-based platforms. As previously described, GBM displays a high degree of both intra-tumoral and inter-tumoral heterogeneity regarding the spatial distribution of neoantigens[12,18]. In this study, we found that although most variants are clonal across multiregional samples, there is an important population of subclonal neoantigens that can drive an immunogenic response, suggesting that a multiregional sampling approach may yield more potent vaccines by more comprehensively targeting spatially distributed neoantigens. DNA vaccine platforms are ideal for accommodating these large numbers of neoantigens.

Neoantigen identification and vaccine production are key rate-limiting steps that could limit the feasibility of a personalized vaccination approach in aggressive malignancies such as GBM. As such, we reasoned that a reasonable time to begin administration of the vaccine would be 4 weeks after completion of radiotherapy, when maintenance therapy (chemotherapy and tumor-treating fields) would typically be started. Unfortunately, in this GT-20 trial, the median time from radiation completion to vaccine initiation was 10 weeks. However, in the GT-30 study, biopsy-to-treatment turnaround times of 6–8 weeks were achieved for all 36 treated patients[19] using streamlined next-generation sequencing data, neoantigen identification and increased manufacturing slot availability. A similar logistical pipeline will ensure that all GBM patients start vaccination within 4 weeks after radiation in future studies.

GNOS-PV01 vaccination generated robust T cell responses in both the peripheral circulation and within the tumor microenvironment. Of note, we observed maintenance of T cell reactivity and evolution of T cell clones over time in patients who underwent serial PBMC sampling. This is best exemplified by patient 8, a long-term survivor who developed expansion of a potential tumor-specific T cell clone 2 years after initial vaccination that led to induction of radiographic pseudoprogression. This result emphasizes the critical need for both longer vaccination regimens and early initiation of vaccination by improved streamlining of vaccine manufacturing to allow sufficient time for patients to reach peak reactivity before the risk of recurrence, which is a critical consideration owing to the aggressive nature of GBM.

Prior studies have shown that temozolomide is of little benefit over standard radiation to patients with unmethylated MGMT promoter GBM[3], and more recent trials found that the addition of nivolumab (PD-1 blockade) to radiation also does not improve overall survival in this patient population[4]. With our method of T cell nuclei enrichment for snRNA-seq, we were able to characterize the tumor microenvironment of patients 2 and 9 post vaccination and identify potential biomarkers and predictors of response. Patient 2 did not display a robust intra-tumoral immune response, had no significant changes in T cell infiltration and showed downregulation of both immune activation signatures and antigen presentation signatures, probably as a result of the administration of dexamethasone concurrently with vaccination. This effect of dexamethasone has been previously reported[10] and underscores the need to use steroid-sparing agents, such as bevacizumab, to control symptomatic edema in future vaccine trials. Patient 2 also did not benefit from pembrolizumab administration, probably secondary to the lack of an activated effector T cell population within the tumor and/or the loss of *B2M* expression on tumor cells. By contrast, patient 9 had a strong vaccine-induced immune response and developed symptomatic vasogenic edema, or pseudoprogression, after the initiation of pembrolizumab, suggesting that the vaccine primed the microenvironment to be responsive to PD-1 blockade. It should be noted that this patient ultimately did not live significantly longer than the expected median (14.8 months versus 12 months) owing to the emergence of distant recurrence in the contralateral hemisphere, which led to rapid disease progression and death. Importantly, the primary lesion from which the personalized vaccine was generated never showed evidence of recurrence after receiving pembrolizumab.

In summary, this study demonstrates that personalized neoantigen DNA-based vaccines can provide a potential adjuvant therapeutic option for patients with GBM, with encouraging outcomes as demonstrated by one-third of patients surviving 24 months or longer. We show that vaccination may prime a T cell or tumor microenvironmental state that permits responsiveness to PD-1 blockade therapy. However, given the rapid clinical decline that can occur in this patient population, early introduction of PD-1 blockade in concert with neoantigen vaccine therapy may be needed. Indeed, the GT-20 cohort reflects the known aggressive nature of MGMT unmethylated GBM. Three patients were ultimately determined to have disease progression on MRI before vaccine initiation (patients 1, 2 and 9). Patient 2 underwent consolidative laser interstitial thermal therapy before receiving the vaccine, while patients 1 and 9, thought to have radiation-induced pseudoprogression, proceeded with vaccine treatment before the next interval MRI confirmed true disease progression. Additionally, two patients (3 and 4) presented with leptomeningeal disease at the time of recurrence and rapidly succumbed to disease progression. Regardless, the observation that GNOS-PV01 treatment led to the induction of tumor neoantigen-specific T cell responses in all the evaluated patients, and that the elicited T cells are $CD8^+$ T cells with an effector phenotype, removes the uncertainty around reliably inducing T cells and enables the systematic evaluation and interpretation of clinical outcomes. The induction of $CD8^+$ T cells with an activated, cytolytic effector phenotype that traffics to the tumor tissue makes the DNA

vaccine platform well-suited to systematically evaluate the contribution of combinatorial PD-1 blockade in the future, as was done in the GT-30 study for patients with advanced liver cancer[19]. As such, these observations served as the rationale for an ongoing phase 1 clinical trial (ClinicalTrials.gov: NCT05743595) to assess the safety, feasibility and effectiveness of a personalized neoantigen-based DNA vaccine in combination with PD-1 blockade therapy for patients with newly diagnosed MGMT promoter unmethylated GBM.

Methods

Study design and overview

This study was registered on ClinicalTrials.gov as NCT04015700 and was conducted in accordance with the Declaration of Helsinki and good clinical practice guidelines. The study was approved by the Institutional Review Board at Washington University School of Medicine, and safety was monitored by the Siteman Cancer Center of Washington University School of Medicine Quality Assurance and Safety Monitoring Committee. The study protocol is included in the Supplementary Information. The study was preregistered on 11 July 2019. All patients signed informed consent to an institutional tissue banking protocol and the study protocol, both of which were approved and monitored by the Institutional Review Board at Washington University School of Medicine. There was no selection bias in the study design. No compensation was provided. Sex was self-reported. Sex was not considered in the study design, given the small sample size. However, there was no discrimination based on sex, age or race in inclusion. The patient population reflects the natural prevalence of the disease. The trial was offered to all patients being evaluated for GBM at Washington University School of Medicine, and patients were sequentially enrolled between 21 July 2020 and 1 December 2021. Patients were screened for inclusion following surgery and after determination of methylation status, but before next-generation sequencing, radiation and vaccine manufacturing. Key inclusion criteria required participants to be aged 18 years or older, have a newly diagnosed central nervous system World Health Organization grade 4 GBM and demonstrate MGMT unmethylated status based on a Clinical Laboratory Improvement Amendment-certified assay. All enrolled patients were IDH wildtype as determined by next-generation sequencing. All patients in the final cohort ($n = 9$) received the vaccine. None of the consented patients dropped out of the trial before the vaccine was administered. Systemic corticosteroid therapy (dexamethasone) was permitted at a dosing of no greater than 4 mg per day on the day of vaccine administration and was used for patient 2.

At the time of initial surgical resection, tumor tissue was sampled from two to four spatially distinct regions and flash-frozen in individual vials as previously described[12,18]. To summarize, once the tumor was extracted by the surgeon, punch biopsies were taken from two to four (depending on tumor size) spatially distinct regions. Punch biopsies were selected based on visual inspection, with the goal of selecting regions far apart from each other without specific measurements obtained. Peripheral blood was also collected at the time of initial tumor resection as previously described[12] to serve as a normal DNA comparator. After patients recovered from surgery, they underwent a course of 6 weeks of intensity-modulated radiotherapy in accordance with standard-of-care guidelines. However, as with our previous peptide vaccine clinical trial[12], patients did not receive standard-of-care concurrent or adjuvant temozolomide owing to a demonstrated lack of efficacy and potential immunosuppressive side effects that may hinder the effects of the vaccine[4]. Each patient's personalized neoantigen DNA vaccine was manufactured during their course of radiation. Tumor-treating fields were permitted in the study as a guideline-directed adjuvant therapy beginning 4 weeks after radiation[32,33]. Three patients elected to pursue tumor-treating fields (Table 1). About 4 weeks after intensity-modulated radiotherapy completion, patients were eligible to receive the priming phase of the vaccine, which entailed a dose given on days 1, 22 and 43 of cycle 1, followed by a dose given on day 1 of each 9-week cycle (boosting phase). The use of PD-1 blockade (pembrolizumab) upon disease progression was permitted. Each personalized neoantigen DNA vaccine (GNOS-PV01), a DNA plasmid expressing up to 40 tumor-specific neoantigens, was co-administered with an adjuvant plasmid encoding IL-12 (INO-9012) using a CELLECTRA 2000 device as previously described[19,34] (all supplied by Geneos Therapeutics). Data collection and analysis were not performed blind to the conditions of the study.

WES and variant calling

WES was performed by the IGM Genomic Services Lab of the Abigail Wexner Research Institute at Nationwide Children's Hospital. Exome sequencing libraries were prepared as previously described for blood and tumor samples[12]. In brief, hybrid capture-based target enrichment was performed using the xGen Exome Research Panel (10005133) combined with the Cancer-Enriched Panels-Tech Access panel (Integrated DNA Technologies). Libraries were then generated using the NEBNext Ultra II FS Kit (New England BioLabs), and paired-end 151 bp reads were sequenced on the NovaSeq6000. We aimed for 100× coverage for blood (we averaged 277× coverage; range, 214–359×) and 250× coverage for tumor samples (we averaged 257× coverage; range, 204–323×). Reads were aligned to the human reference genome build GRCh38, and secondary analyses, including TMB, were performed using our previously published pipeline[35]. Somatic variants were called using MuTect2 (RRID:SCR_000559) and filtered as previously described[12], including a minimum tumor variant allele frequency of ≥2% and gene location within a coding or splice site (<3 bp) region. Integrated Genomics Viewer was used to manually review all variants that passed initial filtering. TMB is additionally reported as measured by FoundationOneCD$_x$ sequencing of the pre-vaccination tumor specimen from each patient that was sent to clinical pathology for diagnostic evaluation (not multi-sector sampled).

Neoantigen prediction, vaccine design and delivery

Clinical HLA class I typing was performed to two-field resolution by Histogenetics using normal comparator peripheral blood obtained at the time of initial surgery. Neoantigens were predicted using pVAC-seq as previously described[12]. In summary, variant call format files for the patient's tumor region were used as input for a containerized version of pVACtools[21] to predict candidate neoantigens[36]. Peptide or MHC binding affinity predictions with class I algorithms NetMHC and NetMHCpan were performed using the 'pvacseq run' submodule. Consistent with our previous trial[12], to be considered for inclusion in the vaccine, candidate neoantigens required WES analysis validation, a best mutant $IC_{50} < 500$ nM, an RNA TPM of >1 and (tumor RNA depth × tumor RNA variant allele frequency) of ≥3. Up to 40 of the top-validated neoantigens for each patient were included in their final vaccine. Each neoantigen contained a CD8 epitope with a somatic mutation and its flanking sequence so that each is about 33 amino acids in length. Patient-specific neoantigen-encoding expression cassettes were designed to consist of a string of neoantigens separated by synthetic furin cleavage sites for efficient epitope processing and presentation[23,37]. The DNA sequences encoding the assembled neoantigens were optimized, synthesized and subcloned into the vaccine expression vector pGX0001 (GenScript)[19,34]. All vaccine plasmids were designed and manufactured under GMP (Good Manufacturing Practices) compliance in collaboration with Geneos Therapeutics and the Biologic Therapy Core Facility at Siteman Cancer Center of Washington University School of Medicine.

As previously described[19,34], the plasmid formulation is devoid of lipopolysaccharides or any potential adjuvants or innate response agonists (such as toll-like receptors). The GMP-manufactured plasmid is formulated in 1× SSC buffer (150 mM sodium chloride, 15 mM sodium citrate, pH 7.0). At each vaccination timepoint, each patient received

one injection of 1 mg of GNOS-PV01 and 1 mg of INO-9012 into the deltoid or lateralis muscle by intramuscular injection, followed by electroporation using the CELLECTRA 2000 electroporation device (Inovio Pharmaceuticals). The CELLECTRA 2000 device is a system indicated for use to enhance the uptake and expression of plasmid-based biologics to enhance vaccine efficacy. The plasmid is delivered separately through intramuscular injection, in the area delineated by the electrodes immediately before the electroporation treatment. The electroporation is accomplished through a sterile, disposable 5-electrode array attached to an applicator. The CELLECTRA 2000 device delivers three pulses, and each pulse lasts 52 ms in duration.

Bulk RNA-seq analysis and immunocyte deconvolution

Bulk RNA-seq was performed by the IGM Genomic Services Lab of the Abigail Wexner Research Institute at Nationwide Children's Hospital. RNA-seq libraries were prepared as previously described for tumor samples[12]. In brief, tumor RNA was DNase-treated and ribodepleted before library construction using the NEBNext Ultra II Directional RNA library kit for Illumina (New England BioLabs). Paired-end 151 bp reads were sequenced on the NovaSeq6000 at a minimum of 80 million reads per sample. Reads were aligned to the human reference genome build GRCh38 using a custom in-house pipeline and the splice-aware aligner STAR (RRID:SCR_004463). The Salmon tool (RRID:SCR_017036) was used to quantify transcript abundance. Neoantigen expression was plotted in R (v.4.3.3) using the pheatmap package (RRID:SCR_016418). For HLA allele expression analysis, reads were aligned to the human HLA nucleotide reference (IPD-IMGT/HLA Database). Immunocyte deconvolution was performed using the publicly available algorithm CIBERSORTx[20] and the human LM22 signature matrix reference (RRID:SCR_016955) as previously described[12]. Relative immunocyte proportions for patients 2 and 9 were reported as percentages and plotted in R (v.4.3.3) using ggplot2 (RRID:SCR_014601).

Volumetric calculations

An independent reviewer performed volumetric measurements on available pre-operative and first available post-operative MRIs visualized using Sectra IDS7. Individual regions of interest were manually defined using the Sectra Area ROI tool, summed across all slices, then multiplied by the slice thickness to determine the volume of non-enhancing (T2 FLAIR) or enhancing (post-contrast T1) volumes.

Immunohistochemistry

Pre-GNOS-PV01 and post-GNOS-PV01 tissue slides from patients 2, 8 and 9 with the highest density of inflammatory cells were stained with hematoxylin and eosin for histological assessment as previously described[12]. Immunohistochemistry for CD8 (Ventana, SP57 clone, prediluted) and CD3 (Ventana, 2GV6 clone, prediluted) was performed on paired tissue slides using the Ventana IHC autostaining platform. Three CD8 and CD3 hotspot areas (0.22 mm^2) were selected and manually counted. Data was graphed using GraphPad Prism (v.10). A two-tailed, unpaired *t*-test was performed to determine statistically significant ($P < 0.05$) differences between mean staining density pre GNOS-PV01 and post GNOS-PV01.

Peptides

For each patient, peptides specific for all neoantigens encoded in the patient-specific DNA vaccine were synthesized from GenScript and used for immune monitoring[19]. Each neoantigen peptide pool (1 mg ml^{-1}) consists of four peptides containing 15 amino acids overlapping by eight amino acids, representing the entire 33-mer neoepitope and a 9-mer predicted CD8 epitope. To make two large peptide pools covering all vaccine-encoded patient-specific neoepitopes, all peptides were pooled at a concentration of 1 mg ml^{-1} into two pools, covering the first half (pool 1) and the second half (pool 2) of vaccine-encoded neoepitopes, respectively.

IFNγ ELISpot assay

The ELISpot assay was performed (FlowMetric) using the standard ELISpot protocol[38] as previously described[19]. Single neoantigen pools were used as the stimulating antigens to detect individual neoantigen-specific responses. Two large peptide pools (pool 1 and pool 2; Supplementary Table 6) were used to detect the total neoantigen-specific responses. A T cell response to a specific neoantigen at a timepoint was considered a positive response if it exceeded five spot-forming units per 10^6 PBMCs and was at least twofold and two standard deviations above the corresponding unstimulated control. A positive neoantigen was counted if it resulted in a positive ELISpot response as defined above at any timepoint. Upon determination of a positive response, the background-subtracted responses for each positive epitope at pre-treatment and on-treatment timepoints were summed to determine the cumulative ELISpot response for that timepoint. The 'best' cumulative response (highest magnitude) for each patient across the available on-treatment timepoints was used as the post-vaccination response for each patient. Data were graphed in GraphPad Prism (v.10).

In vitro stimulation and intracellular cell staining

Intracellular cell staining was performed as previously described[19] using the following markers: CD107A–APC (clone H4A3, Biolegend; 1:200), CD3-BV711 (clone UCHT1, BD Biosciences; 1: 40), CD4-BUV395 (clone RPA-T4, BD Biosciences; 1:100), CD8-BUV805 (clone RPA-T8, BD Biosciences; 1:20), CD69-BV421 (clone FN50, BD Biosciences; 1:20), CD137-BV605 (clone 4B4-1, Biolegend; 1:20), PD-1-PE (clone EH12.1, BD Biosciences; 1:5), IFNγ-BV786 (clone 4S.B3, BD Biosciences; 1:20), IL-2-FITC (clone MQ1-17H12, BD Biosciences; 1:20), Ki67-AF700 (clone B56, BD Biosciences; 1:20), GranzymeA-PerCP/Cy5.5 (clone CB9, Biolegend; 1:20), Perforin-PE/Dazzle594 (clone dG9, Biolegend; 1:20) and TNF-α-PE/Cy7 (clone MAb11, BD Biosciences; 1:20). The gating strategy is shown in Extended Data Fig. 3a. Prepared samples were acquired on the LSRFortessa (BD Biosciences) using FACSDiva software (v.8.0.1). Acquired data were analyzed using FlowJo (v.10.4). Data were graphed in GraphPad Prism (v.10). An unpaired *t*-test with a Gaussian distribution was performed to determine statistical significance ($P < 0.05$).

TCR repertoire sequencing

As previously described[12], genomic DNA from peripheral blood and tumor regions pre GNOS-PV01 and post GNOS-PV01 for patients 2, 8 and 9 were submitted to Adaptive Biotechnologies for human TCR beta chain targeted immunosequencing. Analysis was performed using the immunoSEQ Analyzer 3.0 (Adaptive Biotechnologies). To screen for potentially expanded known viral-reactive T cell clones, we used the publicly available TCRMatch database from the Immune Epitope Database and Analysis Resource to screen for known paired antigen targets. TCRMatch scores range between 0 and 1, with 1 representing an exact match with the input CDR3β sequence. A threshold of ≥0.97 was used as recommended by the program[26]. T cell clone frequency was plotted using ggplot2 (RRID:SCR_014601) in R (v.4.3.3).

snRNA-seq

Nuclei were isolated from frozen tumor sections (25–50 mg in size) from patient 2 (pre-GNOS-PV01 region three and post-GNOS-PV01 tumor resection) and patient 9 (pre-GNOS-PV01 region two and post-GNOS-PV01 tumor resection) following the 10× Chromium Nuclei Isolation Kit Sample Prep User Guide (CG000505 Rev A). To enrich for T cells, nuclei were stained with 5 µl (stock 0.5 mg ml^{-1}) of Alexa Fluor 488 anti-NFATc1 antibody (Biolegend 649604, clone 7A6) per 1 ml of Wash and Resuspension Buffer for 30 min in the dark at 4 °C. To minimize sample loss, we did not perform a wash after the incubation. A total of 10 µl of 7-AAD (ThermoFisher Scientific A1310), a nucleic acid dye that intercalates into double-stranded DNA, was added to the sample before loading onto the BigFoot cell sorter running Sasquatch

(v.1.19.13) software (ThermoFisher Scientific). Nuclei were gated on single cells and then on 7-AAD positivity, and then a liberal Alexa Fluor 488 gate (10^2) was set to initially sort about 14,000 nuclei. This initial liberal gate was applied to ensure that we captured T cells but also other immunocytes, microenvironment and tumor cells. We then moved the Alexa Fluor 488 gate to 10^3 to enrich for the T cells and sorted up to 2,000 additional nuclei with this stringent gate. A maximum total of 16,000 sorted nuclei was sorted directly into 10× Genomics Master Mix and loaded onto a Next GEM Chip K. The Chromium Next GEM Single Cell 5′ v2 (Dual Index) User Guide (Rev E) was then followed according to the manufacturer's recommendations. Gene expression libraries were sequenced on the NovaSeq6000 with a run recipe of 26 × 10 × 10 × 90 targeting 500 million reads per sample (50,000 reads per cell; estimated 10,000 cells per sample). Each tumor region was prepared in biological replicate.

BCL files were converted to FASTQ files using the Cell Ranger (v.7.1.0) mkfastq pipeline. Cell Ranger (v.7.1.0) multi was used with default settings to align reads to the human genome reference GRCh38 and to perform filtering, barcode counting and unique molecular identifier counting. Seurat (v.5)[39] in R (v.4.3.3) was used for analysis following the standard workflow. Samples were filtered for any nuclei that had the following: nFeature less than 1,000 or more than 6,000, nCount greater than 25,000 and mitochondrial reads greater than 5%. All samples (pre-GNOS-PV01 and post-GNOS-PV01 biological replicates from patients 2 and 9) were log-normalized and integrated using the Harmony package[40]. Cell types were annotated using the GBmap ref. 28 Seurat object using the FindTransferAnchors function. T cells were subset, and samples were re-integrated using Harmony[40]. Subtyping was performed using key cell type markers[27]. ggplot2 (RRID:SCR_014601) was used for plotting. Differential expression was performed using the FindMarkers function in Seurat (v.5)[39] with min.pct set to 0.1 and logfc. threshold set to 0.25. Differentially expressed genes were filtered for $P_{adj} < 0.05$. GSEA was performed using fgsea[41] and the Molecular Signatures Database (MSigDB) Gene Ontology Human Biological Process ref. 42. Pathways were filtered for $P_{adj} < 0.05$. Statistical significance for gene expression comparisons plotted in boxplots was calculated across timepoints using an unpaired two-tailed Wilcoxon rank test.

Statistical analysis

No statistical methods were used to pre-determine sample size; sample size was determined based on clinical feasibility and available funding. Data distribution was assumed to be normal, but this was not formally tested.

To measure vaccine-induced T cell response, statistical analyses were performed using a two-tailed unpaired *t*-test with a Gaussian distribution, two-tailed Pearson's test and two-tailed Wilcoxon matched-pairs signed rank test. Given the small sample size and the potential for non-normal distribution of immune response data, non-parametric testing was selected. Data are presented as mean ± s.e.m. unless otherwise indicated.

Sample availability

Additional vials of some sample PBMCs are stored in the Johanns laboratory; they can be made available in the setting of any future research collaborations.

Reporting summary

Further information on research design is available in the Nature Portfolio Reporting Summary linked to this article.

Data availability

De-identified bulk and snRNA-seq and WES for each patient's pre-vaccination tumor samples and post-vaccination tumor resections for patients 2, 8 and 9 are publicly available for download. Bulk and snRNA-seq gene expression data have been deposited in the NCBI Gene Expression Omnibus (GEO) and are accessible through accession numbers GSE292045 and GSE292046, respectively. WES data have been deposited in the NCBI Sequence Read Archive and are available through accession number SRP570525 and BioProject accession number PRJNA1236343. Bulk TCR-seq data have been deposited into the Adaptive Biotech immuneACCESS database (https://clients.adaptivebiotech.com/pub/Garfinkle-2026-nc) and are accessible through GEO accession number GSE327062. The study protocol is included in the Supplementary Information. Additional participant data can be made available upon request. The remaining data are available within the article, Supplementary Information or Source Data files and/or from the corresponding author upon request. Source data are provided with this paper.

Code availability

Code used for the analyses presented in this publication is available at https://github.com/miller-genomics-lab/GT20_GBM_DNA_Vaccine.

References

1. Stupp, R. et al. Radiotherapy plus concomitant and adjuvant temozolomide for glioblastoma. *N. Engl. J. Med.* **352**, 987–996 (2005).
2. Pouyan, A. et al. Glioblastoma multiforme: insights into pathogenesis, key signaling pathways, and therapeutic strategies. *Mol. Cancer* **24**, 58 (2025).
3. Hegi, M. E. et al. *MGMT* gene silencing and benefit from temozolomide in glioblastoma. *N. Engl. J. Med.* **352**, 997–1003 (2005).
4. Omuro, A. et al. Radiotherapy combined with nivolumab or temozolomide for newly diagnosed glioblastoma with unmethylated MGMT promoter: an international randomized phase III trial. *Neuro. Oncol.* **25**, 123–134 (2023).
5. Lim, M. et al. Phase III trial of chemoradiotherapy with temozolomide plus nivolumab or placebo for newly diagnosed glioblastoma with methylated MGMT promoter. *Neuro. Oncol.* **24**, 1935–1949 (2022).
6. Reardon, D. A. et al. Effect of nivolumab vs bevacizumab in patients with recurrent glioblastoma: the Checkmate 143 phase 3 randomized clinical trial. *JAMA Oncol.* **6**, 1003–1010 (2020).
7. Read, R. D. et al. Glioblastoma microenvironment—from biology to therapy. *Genes Dev.* **38**, 360–379 (2024).
8. Sharma, P. et al. Tumor microenvironment in glioblastoma: current and emerging concepts. *Neurooncol. Adv.* **5**, vdad009 (2023).
9. Chongsathidkiet, P. et al. Sequestration of T cells in bone marrow in the setting of glioblastoma and other intracranial tumors. *Nat. Med.* **24**, 1459–1468 (2018).
10. Keskin, D. B. et al. Neoantigen vaccine generates intratumoral T cell responses in phase Ib glioblastoma trial. *Nature* **565**, 234–239 (2019).
11. Hilf, N. et al. Actively personalized vaccination trial for newly diagnosed glioblastoma. *Nature* **565**, 240–245 (2019).
12. Johanns, T. M. et al. Integrating multisector molecular characterization into personalized peptide vaccine design for patients with newly diagnosed glioblastoma. *Clin. Cancer Res.* **30**, 2729–2742 (2024).
13. Weller, M. et al. Rindopepimut with temozolomide for patients with newly diagnosed, EGFRvIII-expressing glioblastoma (ACT IV): a randomised, double-blind, international phase 3 trial. *Lancet Oncol.* **18**, 1373–1385 (2017).
14. Ahluwalia, M. S. et al. Phase IIa study of SurVaxM plus adjuvant temozolomide for newly diagnosed glioblastoma. *J. Clin. Oncol.* **41**, 1453–1465 (2023).
15. Reardon, D. A. et al. Ltbk-01. Ino-5401 and Ino-9012 delivered intramuscularly (IM) with electroporation (EP) in combination with cemiplimab (Regn2810) in newly diagnosed glioblastoma. *Neuro. Oncol.* **22**, ii237 (2020).

16. Liau, L. M. et al. Association of autologous tumor lysate-loaded dendritic cell vaccination with extension of survival among patients with newly diagnosed and recurrent glioblastoma: a phase 3 prospective externally controlled cohort trial. *JAMA Oncol.* **9**, 112–121 (2023).
17. Mendez-Gomez, H. R. et al. RNA aggregates harness the danger response for potent cancer immunotherapy. *Cell* **187**, 2521–2535.e21 (2024).
18. Schaettler, M. O. et al. Characterization of the genomic and immunologic diversity of malignant brain tumors through multisector analysis. *Cancer Discov.* **12**, 154–171 (2022).
19. Yarchoan, M. et al. Personalized neoantigen vaccine and pembrolizumab in advanced hepatocellular carcinoma: a phase 1/2 trial. *Nat. Med.* **30**, 1044–1053 (2024).
20. Newman, A. M. et al. Determining cell type abundance and expression from bulk tissues with digital cytometry. *Nat. Biotechnol.* **37**, 773–782 (2019).
21. Hundal, J. et al. pVAC-Seq: a genome-guided in silico approach to identifying tumor neoantigens. *Genome Med.* **8**, 11 (2016).
22. de Graaf, J. F. et al. Neoantigen-specific T cell help outperforms non-specific help in multi-antigen DNA vaccination against cancer. *Mol. Ther. Oncol.* **32**, 200835 (2024).
23. Bhojnagarwala, P. S. et al. A synDNA vaccine delivering neoAg collections controls heterogenous, multifocal murine lung and ovarian tumors via robust T cell generation. *Mol. Ther. Oncolytics* **21**, 278–287 (2021).
24. Pham, J. et al. Treatment practices and survival outcomes for IDH-wildtype glioblastoma patients according to MGMT promoter methylation status: insights from the U.S. National Cancer Database. *J. Neurooncol.* **172**, 655–665 (2025).
25. Wick, W. et al. Molecularly matched targeted therapies plus radiotherapy in glioblastoma: the phase 1/2a N^2M^2 umbrella trial. *Nat. Med.* **31**, 3534–3541 (2025).
26. Chronister, W. D. et al. TCRMatch: predicting T-cell receptor specificity based on sequence similarity to previously characterized receptors. *Front. Immunol.* **12**, 640725 (2021).
27. Wang, A. Z. et al. Glioblastoma-infiltrating $CD8^+$ T cells are predominantly a clonally expanded $GZMK^+$ effector population. *Cancer Discov.* **14**, 1106–1131 (2024).
28. Ruiz-Moreno, C. et al. Charting the single-cell and spatial landscape of IDH-wild-type glioblastoma with GBmap. *Neuro. Oncol.* **27**, 2281–2295 (2025).
29. Wu, X. et al. Targeting MHC-I molecules for cancer: function, mechanism, and therapeutic prospects. *Mol. Cancer* **22**, 194 (2023).
30. Zaretsky, J. M. et al. Mutations associated with acquired resistance to PD-1 blockade in melanoma. *N. Engl. J. Med.* **375**, 819–829 (2016).
31. Weber, J. S. et al. Individualised neoantigen therapy mRNA-4157 (V940) plus pembrolizumab versus pembrolizumab monotherapy in resected melanoma (KEYNOTE-942): a randomised, phase 2b study. *Lancet* **403**, 632–644 (2024).
32. Stupp, R. et al. Effect of tumor-treating fields plus maintenance temozolomide vs maintenance temozolomide alone on survival in patients with glioblastoma: a randomized clinical trial. *JAMA* **318**, 2306–2316 (2017).
33. Stupp, R. et al. Maintenance therapy with tumor-treating fields plus temozolomide vs temozolomide alone for glioblastoma: a randomized clinical trial. *JAMA* **314**, 2535–2543 (2015).
34. Yarchoan, M., Hopkins, A. & Jaffee, E. M. Tumor mutational burden and response rate to PD-1 inhibition. *N. Engl. J. Med.* **377**, 2500–2501 (2017).
35. Kelly, B. J. et al. Churchill: an ultra-fast, deterministic, highly scalable and balanced parallelization strategy for the discovery of human genetic variation in clinical and population-scale genomics. *Genome Biol.* **16**, 6 (2015).
36. Richters, M. M. et al. Best practices for bioinformatic characterization of neoantigens for clinical utility. *Genome Med.* **11**, 56 (2019).
37. Duperret, E. K. et al. A synthetic DNA, multi-neoantigen vaccine drives predominately MHC class I $CD8^+$ T-cell responses, impacting tumor challenge. *Cancer Immunol. Res.* **7**, 174–182 (2019).
38. Janetzki, S. et al. Results and harmonization guidelines from two large-scale international Elispot proficiency panels conducted by the Cancer Vaccine Consortium (CVC/SVI). *Cancer Immunol. Immunother.* **57**, 303–315 (2008).
39. Hao, Y. et al. Dictionary learning for integrative, multimodal and scalable single-cell analysis. *Nat. Biotechnol.* **42**, 293–304 (2024).
40. Korsunsky, I. et al. Fast, sensitive and accurate integration of single-cell data with Harmony. *Nat. Methods* **16**, 1289–1296 (2019).
41. Korotkevich, G. et al. Fast gene set enrichment analysis. Preprint at *bioRxiv* https://doi.org/10.1101/060012 (2021).
42. Subramanian, A. et al. Gene set enrichment analysis: a knowledge-based approach for interpreting genome-wide expression profiles. *Proc. Natl Acad. Sci. USA* **102**, 15545–15550 (2005).

Acknowledgements

E.A.R.G. was supported by the Mark Foundation for Cancer Research Momentum Fellowship. M.G.C. received research grants from the National Institutes of Health (NIH) National Institute of Neurological Disorders and Stroke (NINDS) (R01NS117149 and R01NS107833). K.E.M. and E.R.M. were supported by the Nationwide Foundation Pediatric Innovation Fund. Geneos Therapeutics supported R.P.L., J.Y., N.C., A.P.P., S.R., J.P. and N.Y.S and provided research funding for the clinical trial design and protocol development, personalized cancer vaccine design, manufacturing and immune monitoring of patient samples. Additionally, the company supplied pIL-12 doses and CELLECTRA 2000 electroporation devices and disposable arrays for the conduct of the trial. T.M.J. was supported by NIH K12 Award K12CA167540 and The Alvin J. Siteman Cancer Center Investment Program, along with The Foundation for Barnes-Jewish Hospital. G.P.D. was supported by NIH NINDS R01NS112712, The Schnuck Family Fund and The Knight and Christopher Davidson Family Fund. We thank the patients for their participation in the research study and physicians and staff at Barnes-Jewish Hospital and the Department of Neurosurgery at Washington University School of Medicine in St. Louis.

Author contributions

E.A.R.G. and R.P.L. conceived the project and conducted formal analysis, investigation, methodology and visualization, and wrote the original draft of the manuscript. R.C.G. reviewed and edited the manuscript. A.J.L. was responsible for data curation, investigation, formal analysis and project administration. K.F.R., M.D.M., G.S.C. and J.H. performed the investigation and formal analysis. O.H.B. and S.C. conducted formal analysis. S.P.G., N.C., A.P.P., K.S., S.R., J.P., B.J., J.L.C., M.G.C., M.R.C., A.H.K., J.T.W., G.J.Z., J.L.D., C.A.M., O.L.G. and M.G. carried out formal analysis and investigation. J.Y. conducted formal analysis and investigation, and contributed to writing the original draft. J.B.N. developed the methodology. S.A.P. created the visualizations. W.E.G. performed the investigation and provided manufacturing and resources. K.E.M., E.R.M. and G.P.D. supervised the project and contributed to writing, review and editing. N.Y.S. carried out conceptualization, formal analysis, investigation, supervision and editing. T.M.J. contributed to conceptualization, formal analysis, funding acquisition, supervision and writing of the original draft.

Competing interests

R.P.L., J.Y., N.C., A.P.P., S.R., J.P. and N.Y.S are either current or previous full-time employees of Geneos Therapeutics. B.J. has a consultant role for Geneos Therapeutics. O.L.G and M.G. have consultant roles for

the Jaime Leandro Foundation for Therapeutic Cancer Vaccines and Pathfinder Oncology. W.E.G has a consultant role for Jamie Leandro Foundation. The remaining authors declare no competing interests.

Additional information

Extended data is available for this paper at https://doi.org/10.1038/s43018-026-01163-w.

Supplementary information The online version contains supplementary material available at https://doi.org/10.1038/s43018-026-01163-w.

Correspondence and requests for materials should be addressed to Tanner M. Johanns.

Peer review information *Nature Cancer* thanks Annette Molinaro, Michael Platten, Robert Prins and Adam Sonabend for their contribution to the peer review of this work.

Elizabeth A. R. Garfinkle[1], Renzo Perales-Linares[2], Ryan C. Gimple[3], Alexandra J. Livingstone[4], Kaleigh F. Roberts[5], Omar H. Butt[4,6], S. Peter Goedegebuure[6,7], Michael D. McLellan[8], Gue Su Chang[8], Jasreet Hundal[8], Jian Yan[2], Jaye B. Navarro[1], Sophia A. Paxton[1,9], Srestha Chattopadhyay[1,10], Neil Cooch[2], Alfredo Perales-Puchalt[2], Konstantina Stavroulaki[11], Sarah Rochestie[2], Joann Peters[2], Beth Junker[12], Jian L. Campian[13], Milan G. Chheda[3,6], Michael R. Chicoine[14], Albert H. Kim[6,15], Jon T. Willie[15], Gregory J. Zipfel[6,15], Joshua L. Dowling[6,15], Christopher A. Miller[3,8,16], Obi L. Griffith[3,8,16], Malachi Griffith[3,8,16], William E. Gillanders[17], Katherine E. Miller[1,18], Elaine R. Mardis[1,18], Niranjan Y. Sardesai[2,21], Gavin P. Dunn[19,21] & Tanner M. Johanns[4,6,20,21] ✉

[1]The Steve and Cindy Rasmussen Institute for Genomic Medicine, Nationwide Children's Hospital, Columbus, OH, USA. [2]Geneos Therapeutics, Philadelphia, PA, USA. [3]Department of Medicine, Washington University School of Medicine, St. Louis, MO, USA. [4]Division of Medical Oncology, Washington University School of Medicine, St. Louis, MO, USA. [5]Department of Pathology and Immunology, Washington University School of Medicine, St. Louis, MO, USA. [6]The Brain Tumor Center at Siteman Cancer Center, Washington University in St. Louis, St. Louis, MO, USA. [7]Department of Surgery, Washington University in St. Louis, St. Louis, MO, USA. [8]McDonnell Genome Institute, Washington University School of Medicine, St. Louis, MO, USA. [9]Biomedical Sciences Graduate Program, The Ohio State University College of Medicine, Columbus, OH, USA. [10]The Ohio State University, Columbus, OH, USA. [11]Department of Radiation Oncology, Washington University School of Medicine, St. Louis, MO, USA. [12]BioProcess Advantage LLC, Westfield, NJ, USA. [13]Department of Neurology, Mayo Clinic, Rochester, MN, USA. [14]Department of Neurosurgery, University of Missouri, Columbia, MO, USA. [15]Department of Neurosurgery, Washington University School of Medicine, St. Louis, MO, USA. [16]Department of Genetics, Washington University School of Medicine, St. Louis, MO, USA. [17]Department of Surgery, Washington University School of Medicine, St. Louis, MO, USA. [18]Department of Pediatrics, The Ohio State University College of Medicine, Columbus, OH, USA. [19]Department of Neurosurgery, Massachusetts General Hospital, Harvard Medical School, Boston, MA, USA. [20]Andrew M. and Jane M. Bursky Center for Human Immunology and Immunotherapy Program, Washington University School of Medicine, St. Louis, MO, USA. [21]These authors jointly supervised this work: Niranjan Y. Sardesai, Gavin P. Dunn, Tanner M. Johanns. ✉e-mail: tannerjohanns@wustl.edu

https://doi.org/10.1038/s43018-026-01163-w

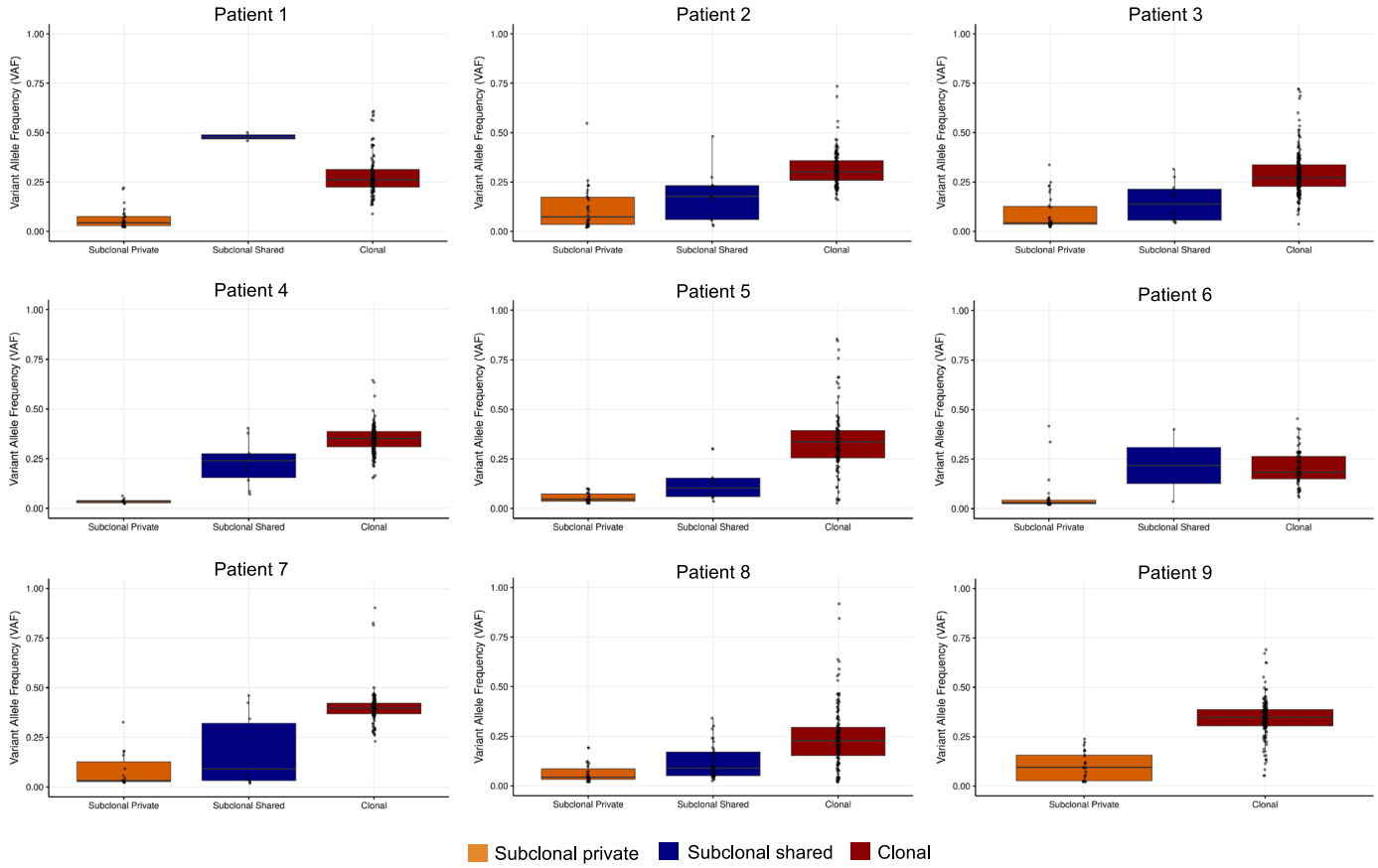

Extended Data Fig. 1 | DNA variant allele frequencies. DNA variant allele frequency (VAF) of variants grouped by regional distribution. Boxes represent the interquartile range (IQR), center line designates the median, whiskers extend to 1.5xIQR, and each dot represents a variant. Variants are called from all pre-GNOS-PV01 tumor samples (n = 3 for all patients except for n = 4 for patient 2).

https://doi.org/10.1038/s43018-026-01163-w

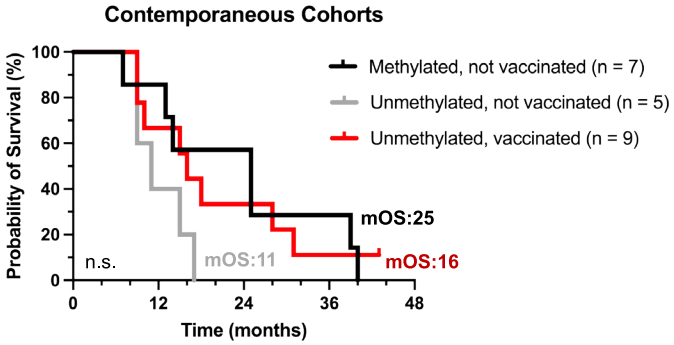

Extended Data Fig. 2 | Survival outcomes. Kaplan-Meyer curve displaying probability of survival over time from diagnosis (in months) for contemporaneous cohorts: MGMT methylated patients (n = 7, black line) and MGMT unmethylated patients (n = 5, grey line) treated with standard of care chemoradiotherapy (temozolomide) compared with MGMT unmethylated patients (n = 9, red line) treated with GNOS-PV01vaccination on the GT-20 trial. Long-rank test was used to calculate statistical significance. Abbreviations: mOS, median overall survival.

https://doi.org/10.1038/s43018-026-01163-w

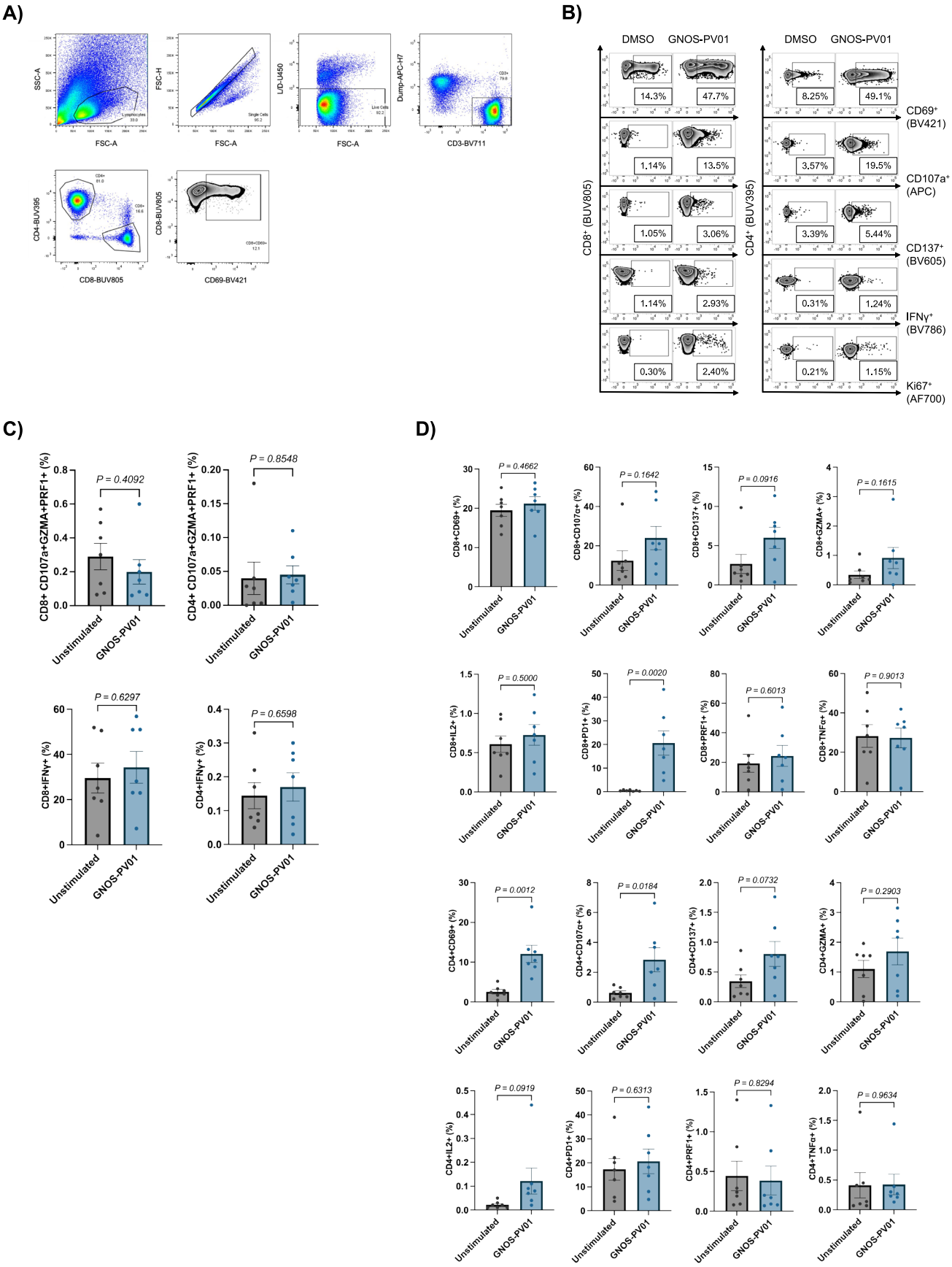

Extended Data Fig. 3 | See next page for caption.

https://doi.org/10.1038/s43018-026-01163-w

Extended Data Fig. 3 | Extended analysis showing GNOS-PV01 drives polyfunctional T cell immunity. A) Gating strategy (left to right). Cells were gated on PBMCs [forward scatter (FSC)-A versus side scatter (SSC)-A], singlets (FSC-A versus FSC-H), live cells (FSC-A versus Live/Dead), lymphocytes (CD3+ versus dump markers), CD8 or CD4 T cells (CD8 versus CD4) and marker- or cytokine-positive populations were quantified within each subset. Boolean gating was performed to define combinatorial expression patterns where indicated. This gating strategy applies to all flow cytometry studies presented in the manuscript. **B**) Representative density plots (patient 7) of the T cell markers CD69, CD107a, CD137, IFNγ, and Ki67 upon stimulation with patient-specific vaccine neoantigen epitope pools. **C-D**) Individual CD4+ or CD8 + T cell markers from PBMCs were evaluated in seven patients (2-8). 2.5×10^5 post-GNOS-PV01 PBMCs from C2D8 for patients 2-7 and C2D1 for patient 8 were cultured in growth media with IL-2, IL-4, and IL-7 and enriched for neoantigen-specific T cells with 10 μg/ml of personalized neoantigen stimuli (GNOS-PV01) or controls (Unstimulated). Cells were then stained intracellularly and with surface marker antibodies for T cell effector markers. Each filled circle represents a patient. Data represent mean ± SEM. *p* value evaluated by two-sided, unpaired t-test with Gaussian distribution.

https://doi.org/10.1038/s43018-026-01163-w

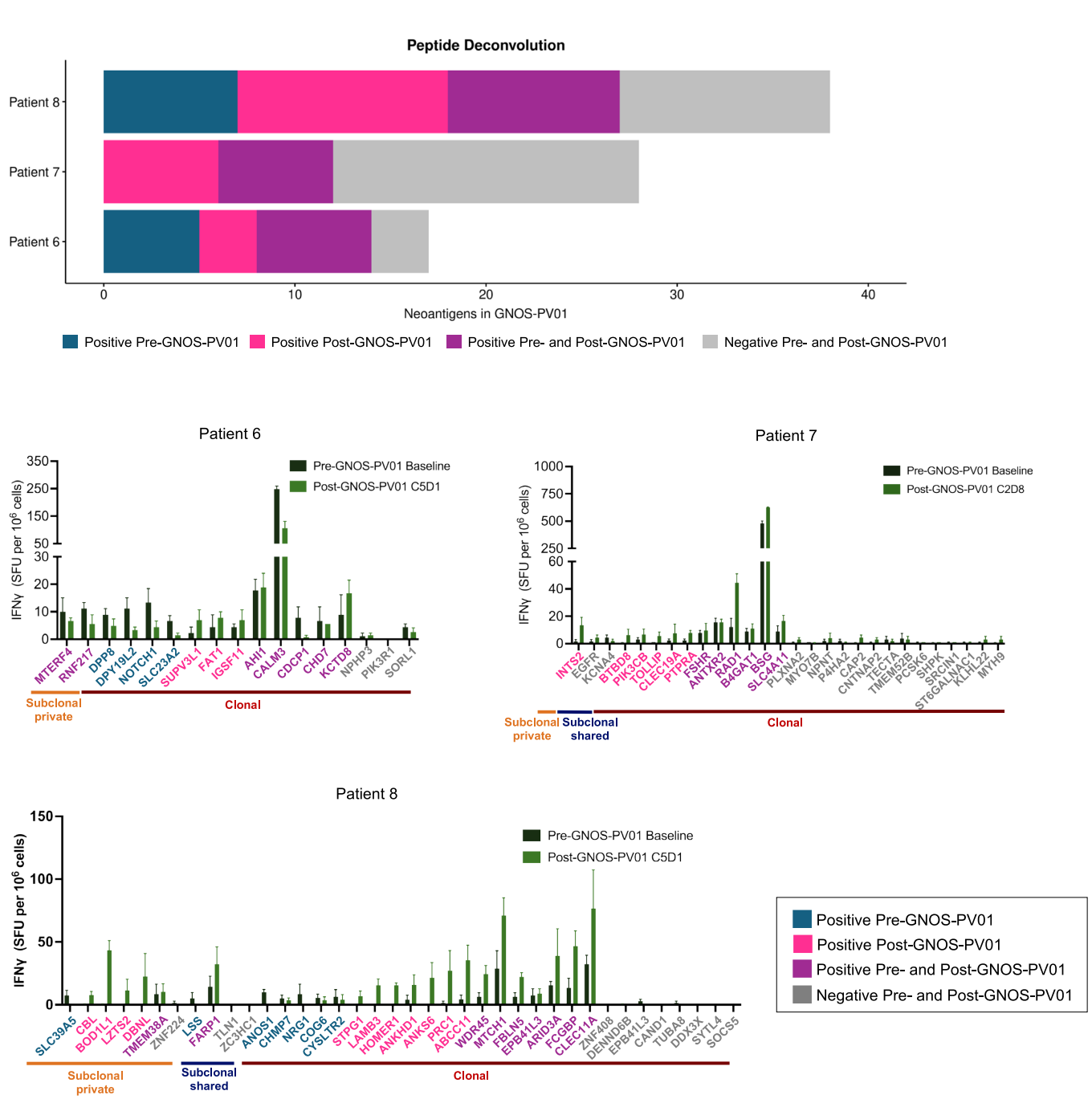

Extended Data Fig. 4 | Peptide deconvolution by IFN-γ ELISpot assay. **A-B**) 3x10^5 PBMCs from patients 6 – 8 per well were stimulated with vaccine-encoded epitopes at the concentration of 10 μg/mL for 18–24 h. Cells were evaluated for the presence of vaccine-induced neoantigen-specific responses prior to (Baseline) and post-GNOS-PV01 vaccination using an interferon IFNγ ELISPOT assay without cytokine stimulation. **A**) Positive neoantigens pre-GNOS-PV01 (teal), positive neoantigens post-GNOS-PV01 (pink), positive neoantigens pre- and post-GNOS-PV01 (purple), and negative neoantigens pre- and post-GNOS-PV01 (grey) are plotted in a summary bar plot for each evaluated patient. **B**) Individual neoantigen responses from peptide deconvolution assay are plotted for each patient. The bar indicates the mean SFU of n = 3 individual technical replicates ± SD per group. Each neoantigen is colored response as described above. Regional distribution (subclonal private, subclonal shared, or clonal) is notated below each neoantigen. Abbreviations: C#D#, cycle # day #, SFU, spot-forming units.

https://doi.org/10.1038/s43018-026-01163-w

A) Patient 2

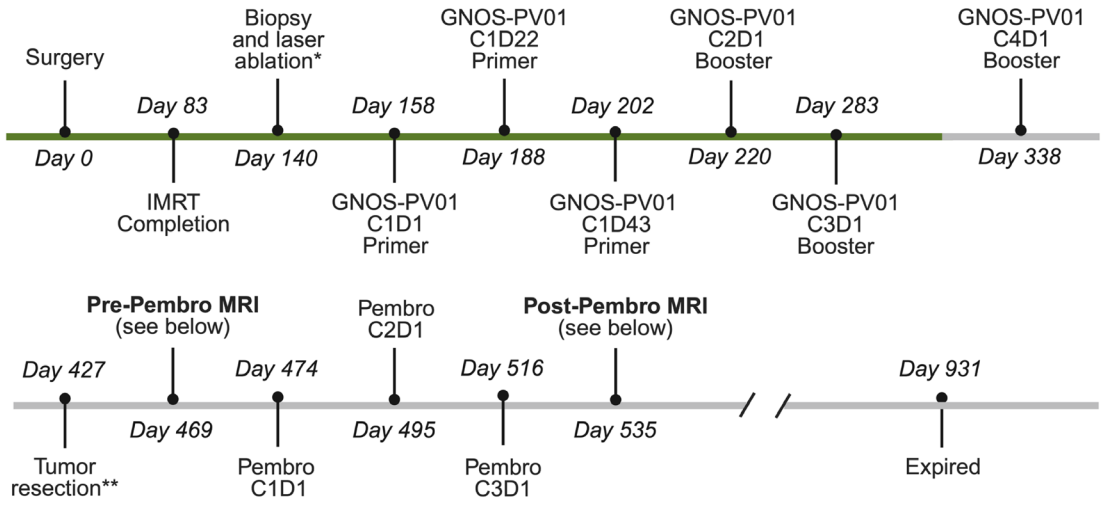

*Minute fragments of high grade glial neoplasm in background of blood clot. Ki67 proliferation rate in the tumor is approximately 10%

**Diffusely infiltrative high-grade glioma with mostly dense cellularity and multifocal palisading necrosis. In addition, prominent bland "radiation necrosis", vasculopathic changes, and chronic inflammatory cell infiltrate are present. Ki-67 proliferation index is estimated to be up to ~25-30% focally. Approximately 50-60% of the current resection is composed of residual/recurrent IDH-wildtype glioblastoma that is mostly "active." Remainder shows treatment effect with predominantly radiation necrosis.

B)

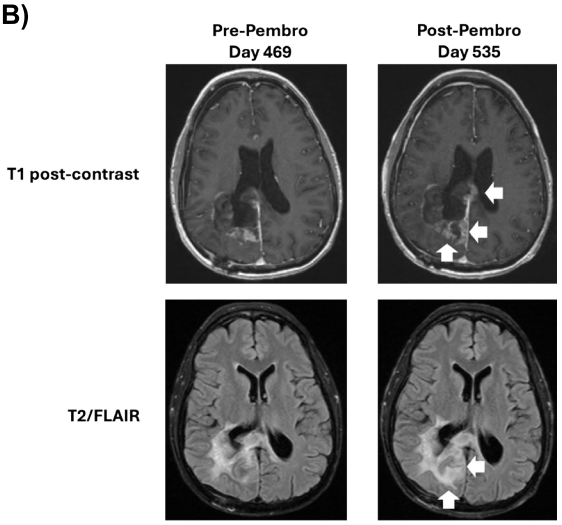

C)

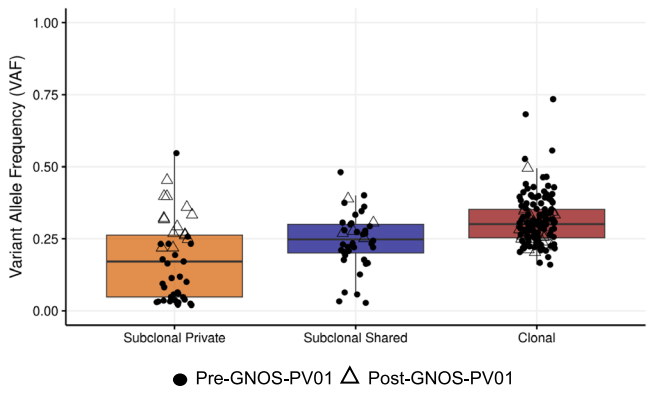

Extended Data Fig. 5 | Patient 2 clinical outcomes. A) Timeline in days displaying clinical events while on the trial from time of initial surgery. **B**) Magnetic resonance imaging (MRI) scans from two post-GNOS-PV01 timepoints. White arrows point to areas of disease progression. **C**) DNA variant allele frequency (VAF) of variants grouped by regional distribution with the inclusion of a post-GNOS-PV01 tumor resection (open triangle symbol). Boxes represent the interquartile range (IQR), center line designates the median, whiskers extend to 1.5xIQR, and each dot represents a variant. Variants are called from all four pre-GNOS-PV01 and single post-GNOS-PV01 sample(s). Abbreviations: IMRT, intensity modulated radiation therapy; C#D#, cycle # day #. **A**) Created in BioRender; Garfinkle, E. https://BioRender.com/whqdak9 (2026).

https://doi.org/10.1038/s43018-026-01163-w

A) Patient 9

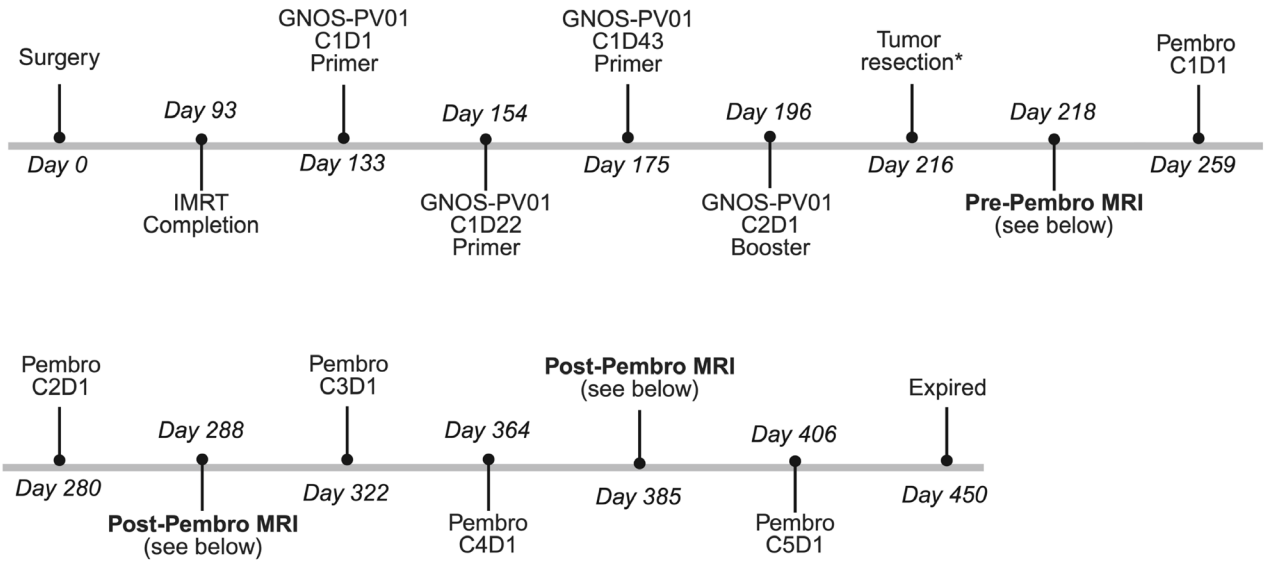

*Areas of residual/recurrent glioma with moderate cellularity and atypia are present. Also present are treatment related changes including bland "radiation" necrosis and vasculopathic changes. Edema is regionally conspicuous. Ki-67 proliferation index is variably increased, estimated up to ~10 to 40% with some contribution by the intermixed immune cells.

B)

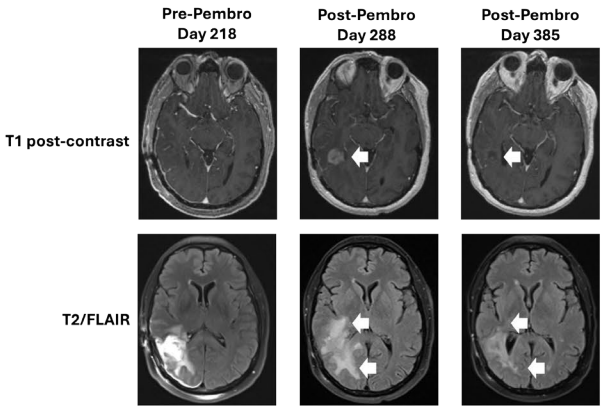

C)

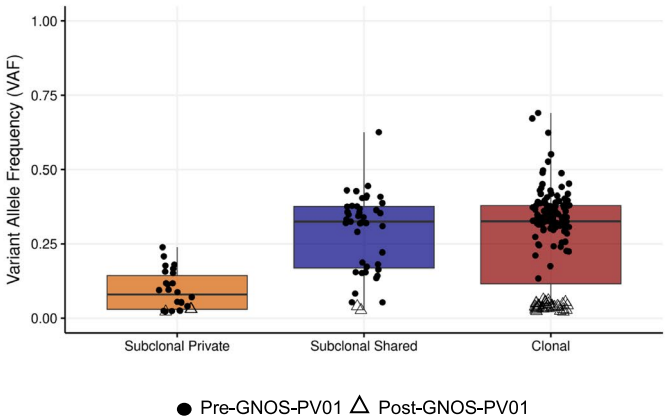

Extended Data Fig. 6 | Patient 9 clinical outcomes. A) Timeline in days displaying clinical events while on the trial from time of initial surgery. **B**) Magnetic resonance imaging (MRI) scans from three post-GNOS-PV01 timepoints. White arrows point to areas of disease progression. **C**) DNA variant allele frequency (VAF) of variants grouped by regional distribution with the inclusion of a post-GNOS-PV01 tumor resection (open triangle symbol). Boxes represent the interquartile range (IQR), center line designates the median, whiskers extend to 1.5xIQR, and each dot represents a variant. Variants are called from all three pre-GNOS-PV01 and single post-GNOS-PV01 sample(s). Abbreviations: IMRT, intensity modulated radiation therapy; C#D#, cycle # day #. **A**) Created in BioRender; Garfinkle, E. https://BioRender.com/u6txxin (2026).

https://doi.org/10.1038/s43018-026-01163-w

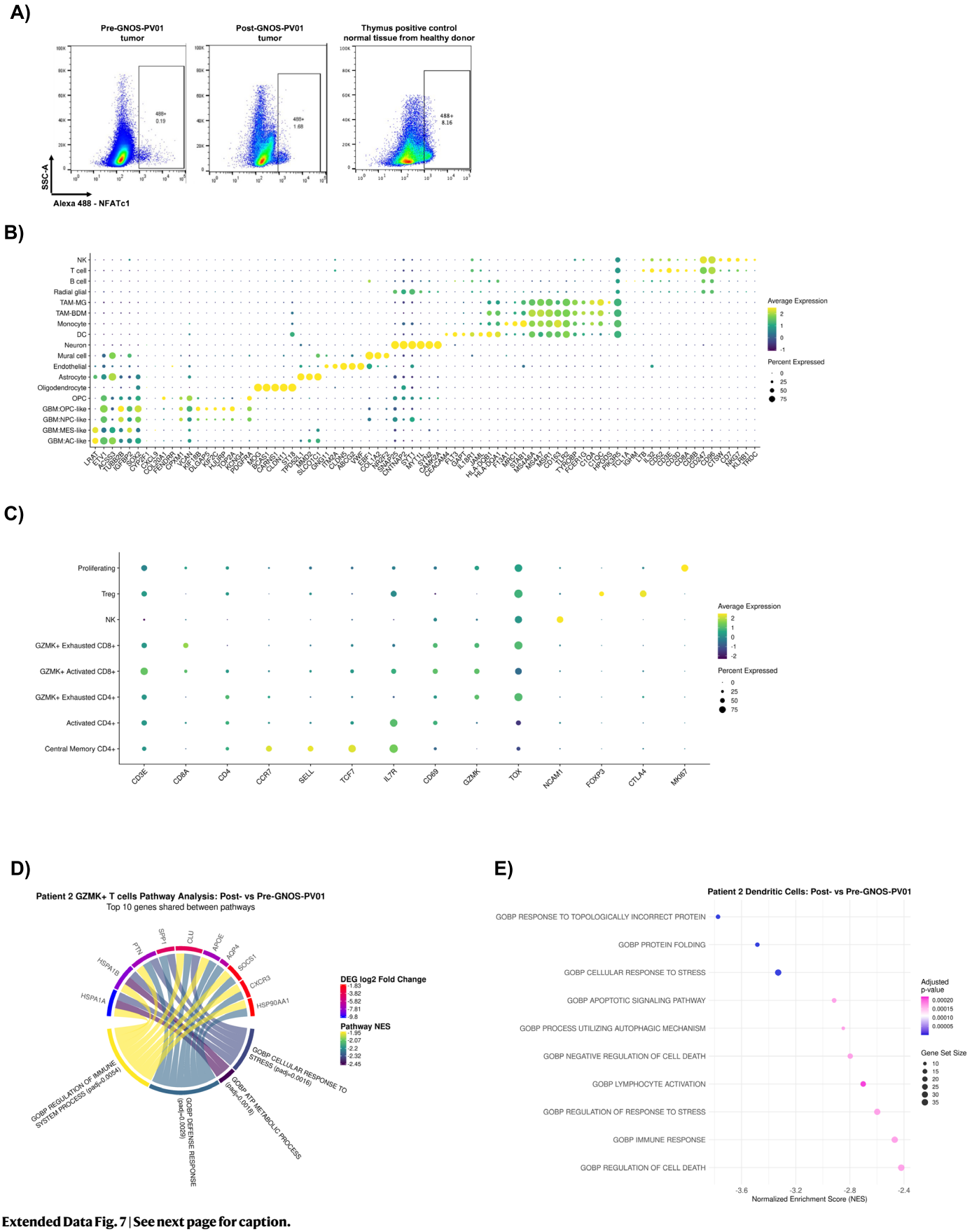

Extended Data Fig. 7 | See next page for caption.

https://doi.org/10.1038/s43018-026-01163-w

Extended Data Fig. 7 | Single nuclei RNA-sequencing (snRNA-seq) uncovers transcriptional changes of GBM infiltrating T and dendritic cells in the post-vaccination tumor immune microenvironment. A) Representative gating strategy for T cell enrichment by NFATc1 nuclear staining. An example pre- and post-GNOS-PV01 sample is shown as well as an example positive control thymus from an unrelated, healthy donor. **B**) Dotplot showing expression of key marker genes for each annotated cell type via the GBmap reference. Data is scaled. **C**) Dotplot showing expression of key marker genes for each annotated T cell subtype. Data is scaled. **D**) GZMK+ activated and exhausted cells were computationally subset and differential expression analysis using the FindMarkers function in Seurat v5 was performed comparing patient 2 post- to pre-GNOS-PV01. Four significant pathways of interest with negative enrichment scores are displayed and colored by their normalized enrichment score (NES). The top ten differentially expressed genes (DEG) shared among the pathways are shown and colored by log2 fold change. Genes contributing to each pathway are connected by chords. **E**) Dendritic cells were computationally subset and differential expression analysis using the FindMarkers function in Seurat v5 was performed comparing patient 2 post- to pre-GNOS-PV01. The top ten significant pathways after gene set enrichment analysis (Gene Ontology Human Biological Processes reference) are displayed in a bubble plot. The size of the circles represents the pathway gene set size and the color of the dots shows the adjusted *p*-value. Differentially expressed genes were identified using a non-parametric Wilcoxon rank-sum test with Benjamini–Hochberg false discovery rate (FDR) correction. Gene set enrichment analysis was performed using a permutation-based enrichment score statistic with FDR adjustment. Abbreviations: GBM, glioblastoma; AC-like, astrocyte-like; MES- like, mesenchymal-like; OPC-like, oligodendrocyte progenitor cell-like; OPC, oligodendrocyte progenitor cell; DC, dendritic cell; TAM- BDM, tumor associated macrophage that originate from bone marrow; TAM-MG, tumor associated macrophage that originate from microglia; NK, natural killer cells; Treg, regulatory T cells.

https://doi.org/10.1038/s43018-026-01163-w

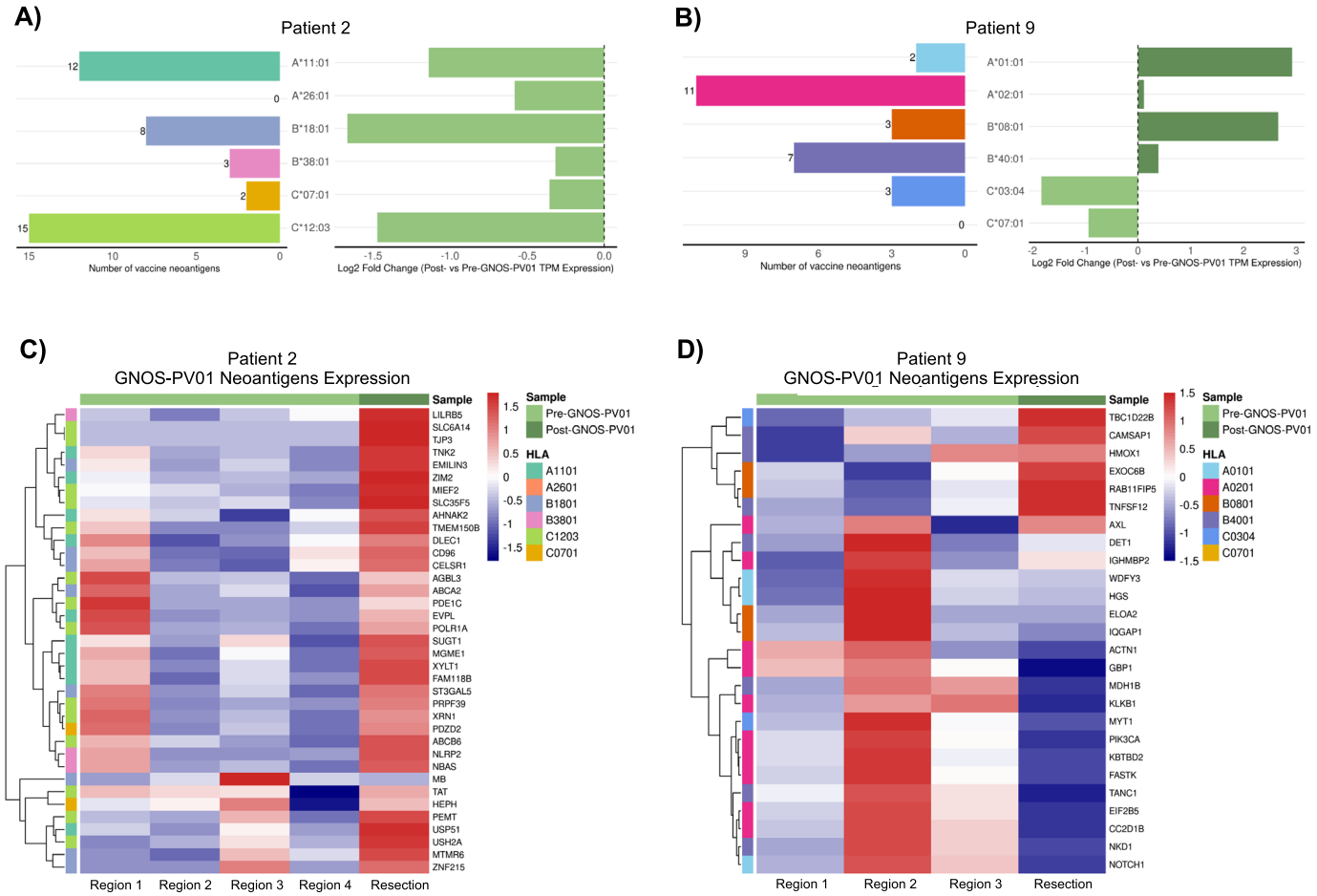

Extended Data Fig. 8 | Bulk and single nuclei RNA-sequencing (snRNA-seq) reveals altered transcriptional states in the GBM microenvironment before and after GNOS-PV01. A-B) Bulk RNA-seq data for **A**) patient 2 and **B**) patient 9 were aligned to the human HLA nucleotide reference (IPD-IMGT/HLA Database). Log2 fold change of post- vs pre-GNOS-PV01 transcripts per million (TPM) expression values were calculated for each patient's HLA alleles and plotted in a bar graph. The number of neoantigens included in each patient's vaccine predicted to be presented by each HLA allele (determined from pVAC-seq) are also plotted in a corresponding bar graph. **C-D**) Bulk RNA-seq data aligned to the human reference genome build GRCh38 was used to plot expression of vaccine neoantigens for **C**) patient 2 and **D**) patient 9 before and after GNOS-PV01. Each row is scaled. The HLA allele predicted to present each neoantigen (determined from pVAC-seq) is annotated on the right of the heatmap.

https://doi.org/10.1038/s43018-026-01163-w

A)

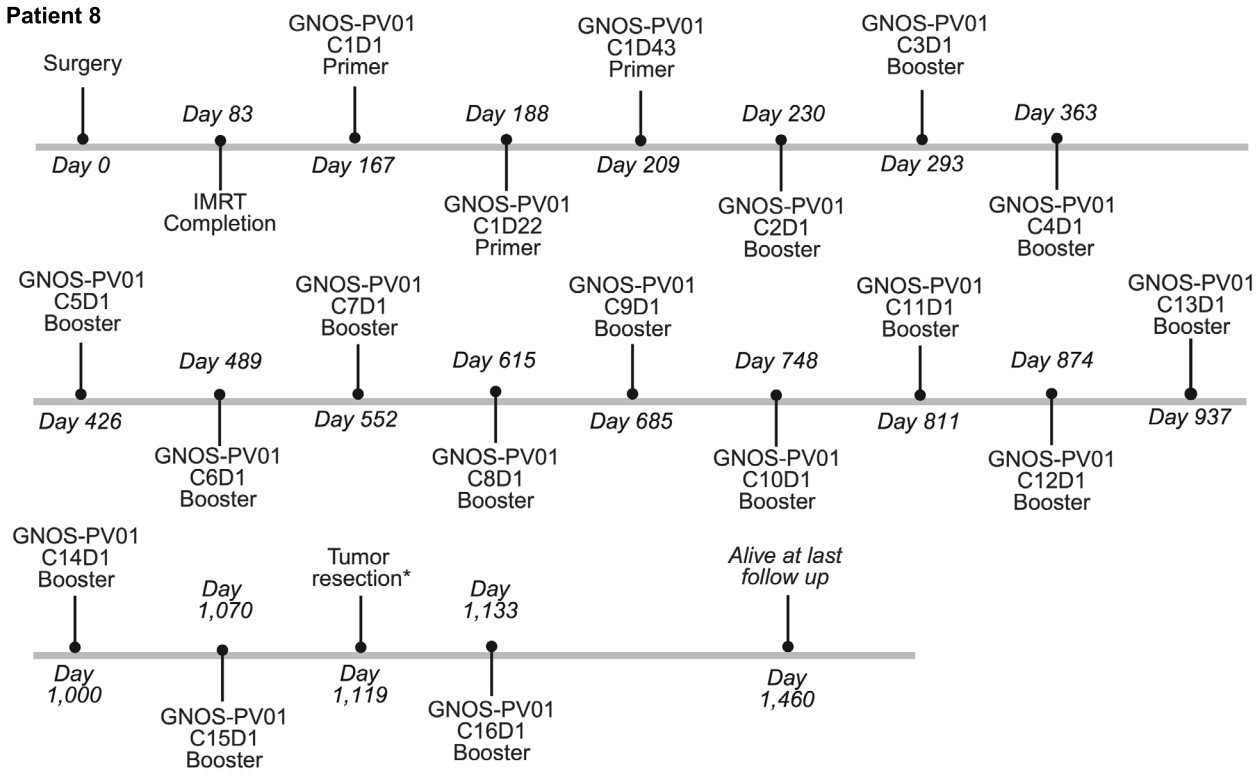

*Pathology showed persistent/residual glioma with treatment effect including areas of radiation necrosis in the background. Some tissue fragments were moderately hypercellular, with immune cells intermixed among an atypical, infiltrative glial population. The atypical cells have moderate nuclear pleomoprhism with scant eosinophilic cytoplasm and mitoses difficult to find. Numerous vessels demonstrate fibrinoid necrosis and there is a rare focus of microvascular proliferation albeit with hyalinization of its walls. Ki-67 proliferation index is variably increased with contribution by the intermixed immune and endothelial cells.

B)

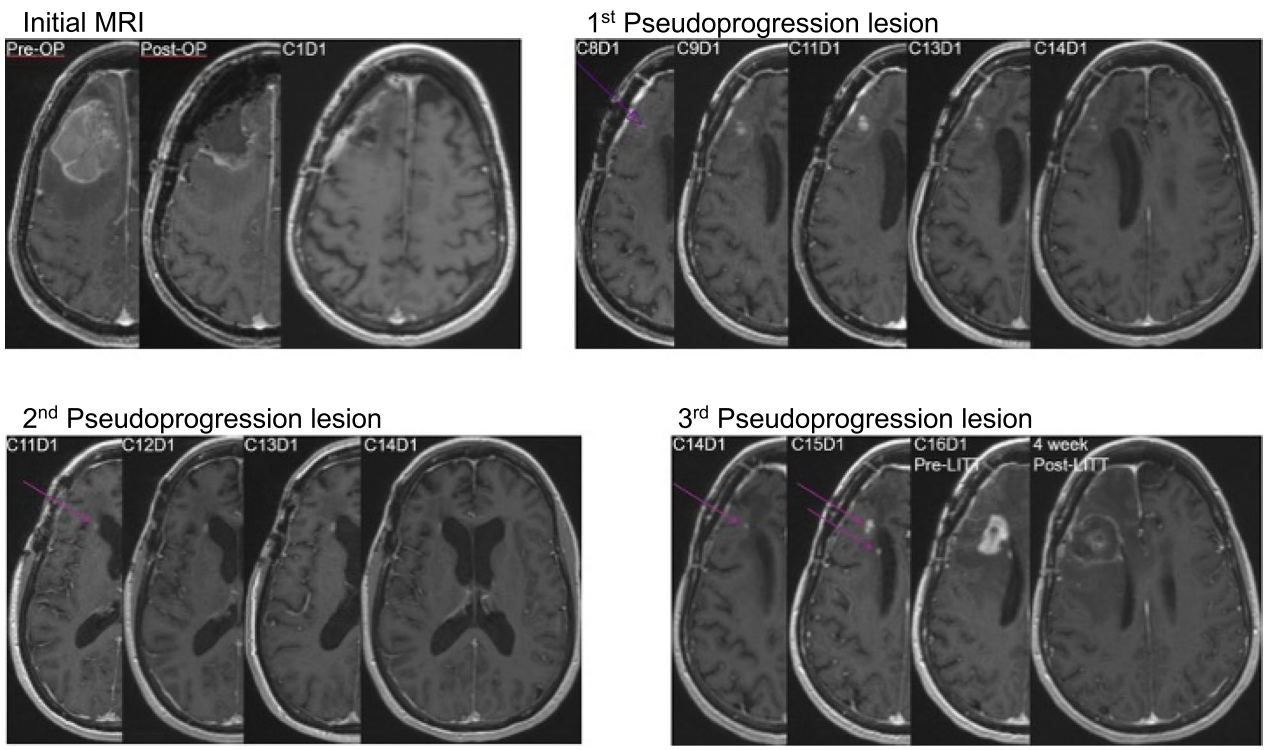

Extended Data Fig. 9 | Patient 8 clinical outcomes. A) Timeline in days displaying clinical events while on the trial from time of initial surgery. **B**) Serial magnetic resonance imaging (MRI) scans showing pseudoprogression and resolution. Abbreviations: IMRT, intensity modulated radiation therapy; C#D#, cycle # day #. **A**) Created in BioRender; Garfinkle, E. https://BioRender.com/kviuyit (2026).

nature portfolio

Corresponding author(s): Tanner M. Johanns

Last updated by author(s): 2026-04-06

Reporting Summary

Nature Portfolio wishes to improve the reproducibility of the work that we publish. This form provides structure for consistency and transparency in reporting. For further information on Nature Portfolio policies, see our Editorial Policies and the Editorial Policy Checklist.

Please do not complete any field with "not applicable" or n/a. Refer to the help text for what text to use if an item is not relevant to your study.
For final submission: please carefully check your responses for accuracy; you will not be able to make changes later.

Statistics

For all statistical analyses, confirm that the following items are present in the figure legend, table legend, main text, or Methods section.

n/a	Confirmed	
☐	☒	The exact sample size (*n*) for each experimental group/condition, given as a discrete number and unit of measurement
☐	☒	A statement on whether measurements were taken from distinct samples or whether the same sample was measured repeatedly
☐	☒	The statistical test(s) used AND whether they are one- or two-sided *Only common tests should be described solely by name; describe more complex techniques in the Methods section.*
☐	☒	A description of all covariates tested
☐	☒	A description of any assumptions or corrections, such as tests of normality and adjustment for multiple comparisons
☐	☒	A full description of the statistical parameters including central tendency (e.g. means) or other basic estimates (e.g. regression coefficient) AND variation (e.g. standard deviation) or associated estimates of uncertainty (e.g. confidence intervals)
☐	☒	For null hypothesis testing, the test statistic (e.g. *F*, *t*, *r*) with confidence intervals, effect sizes, degrees of freedom and *P* value noted *Give P values as exact values whenever suitable.*
☒	☐	For Bayesian analysis, information on the choice of priors and Markov chain Monte Carlo settings
☒	☐	For hierarchical and complex designs, identification of the appropriate level for tests and full reporting of outcomes
☐	☒	Estimates of effect sizes (e.g. Cohen's *d*, Pearson's *r*), indicating how they were calculated

Our web collection on statistics for biologists contains articles on many of the points above.

Software and code

Policy information about availability of computer code

Data collection	N/A
Data analysis	We used the following open-source code for single nuclei RNA-seq analysis: cellranger v7.1.0 mkfastq for BCL to FASTQ and cell ranger v7.1.10 multi for alignment and counts. Seurat v5 in R v4.3.3. was used for downstream analysis. All code is available at: https://github.com/eargarfinkle/GT20_GBM_DNA_Vaccine.

For manuscripts utilizing custom algorithms or software that are central to the research but not yet described in published literature, software must be made available to editors and reviewers. We strongly encourage code deposition in a community repository (e.g. GitHub). See the Nature Portfolio guidelines for submitting code & software for further information.

Data

Policy information about availability of data

All manuscripts must include a data availability statement. This statement should provide the following information, where applicable:

- Accession codes, unique identifiers, or web links for publicly available datasets
- A description of any restrictions on data availability
- For clinical datasets or third party data, please ensure that the statement adheres to our policy

De-identified bulk and single-nuclei RNA-sequencing and whole exome sequencing for each patient's pre-vaccination tumor samples and post-vaccination tumor resections for patients 2, 8, and 9 are publicly available for download. The bulk and single-nuclei RNA-sequencing gene expression data presented in this publication have been deposited in NCBI's Gene Expression Omnibus and are accessible through Gene Expression Omnibus Series accession number GSE292045 (https://www.ncbi.nlm.nih.gov/geo/query/acc.cgi?acc=GSE292045) and GSE292046 (https://www.ncbi.nlm.nih.gov/geo/query/acc.cgi?acc=GSE292046), respectively. The whole exome sequencing data presented in this publication have been deposited in NCBI's Sequence Read Archive and are available through SRA accession number SRP570525 (https://trace.ncbi.nlm.nih.gov/Traces/?study=SRP570525) and BioProject accession number PRJNA1236343 (https://www.ncbi.nlm.nih.gov/bioproject/PRJNA1236343). The bulk TCR-seq data has been deposited into Adaptive Biotech's immuneACCESS database (https://clients.adaptivebiotech.com/pub/Garfinkle-2026-nc) and are accessible through Gene Expression Omnibus Series accession number GSE327062 (https://www.ncbi.nlm.nih.gov/geo/query/acc.cgi?acc=GSE327062). The study protocol is included in the Supplementary Information. Additional participant data can be made available upon request. The remaining data are available within the Article, Supplementary Information or Source Data file and/or from the corresponding author upon request.

Research involving human participants, their data, or biological material

Policy information about studies with human participants or human data. See also policy information about sex, gender (identity/presentation), and sexual orientation and race, ethnicity and racism.

Reporting on sex and gender	The informed consent did not explicitly state sex information would be published. Therefore, we are not reporting each patient's sex but rather presenting at a cohort level. 67% of the cohort was male. Sex was determined by self-report. Sex was not considered in the study design given the small sample size. However, there was no discrimination to sex inclusion either. Instead, patient population reflects the natural prevalence of the disease.
Reporting on race, ethnicity, or other socially relevant groupings	The informed consent did not explicitly state ancestry information would be published. Therefore, we are not reporting each patient's ancestry but rather presenting at a cohort level. 100% of the cohort was Caucasian. Ancestry was determined by self-report. Ancestry was not considered in the study design given the small sample size. However, there was no discrimination to ancestry inclusion either. Instead, the patient population reflects the natural prevalence of the disease.
Population characteristics	All 9 patients who received vaccine and are reported here were adults with newly diagnosed, previously untreated, MGMT unmethylated GBM. The informed consent did not explicitly state age information would be published. Therefore, we are not reporting each patient's age but rather presenting at a cohort level. The median age was 59 (range 54 - 68).
Recruitment	The trial was offered to all patients being evaluated for GBM at Washington University School of Medicine.
Ethics oversight	Institutional Review Board at Washington University School of Medicine.

Note that full information on the approval of the study protocol must also be provided in the manuscript.

Field-specific reporting

Please select the one below that is the best fit for your research. If you are not sure, read the appropriate sections before making your selection.

☒ Life sciences ☐ Behavioural & social sciences ☐ Ecological, evolutionary & environmental sciences

For a reference copy of the document with all sections, see nature.com/documents/nr-reporting-summary-flat.pdf

Life sciences study design

All studies must disclose on these points even when the disclosure is negative.

Sample size	No statistical methods were used to pre-determine sample size, but rather, sample size was determined based on clinical feasibility and available funding.
Data exclusions	No collected data were excluded from the analyses presented in this manuscript. In some cases there was not sufficient material from each patient for each experiment. When this is the case, it is noted in the manuscript.
Replication	Replicates are noted in the manuscript. Functional assays were replicated 3 times and single nuclei RNA-sequencing was done twice. All replicates were successful and included.
Randomization	This is a non-randomized single arm study.
Blinding	Data collection and analysis were not performed blind to the conditions of the study.

Behavioural & social sciences study design

All studies must disclose on these points even when the disclosure is negative.

Study description	
Research sample	
Sampling strategy	
Data collection	
Timing	
Data exclusions	
Non-participation	
Randomization	

Ecological, evolutionary & environmental sciences study design

All studies must disclose on these points even when the disclosure is negative.

Study description	
Research sample	
Sampling strategy	
Data collection	
Timing and spatial scale	
Data exclusions	
Reproducibility	
Randomization	
Blinding	

Did the study involve field work? ☐ Yes ☐ No

Field work, collection and transport

Field conditions	
Location	
Access & import/export	
Disturbance	

Reporting for specific materials, systems and methods

We require information from authors about some types of materials, experimental systems and methods used in many studies. Here, indicate whether each material, system or method listed is relevant to your study. If you are not sure if a list item applies to your research, read the appropriate section before selecting a response.

Materials & experimental systems

n/a	Involved in the study
☐	☒ Antibodies
☒	☐ Eukaryotic cell lines
☒	☐ Palaeontology and archaeology
☒	☐ Animals and other organisms
☐	☒ Clinical data
☒	☐ Dual use research of concern
☒	☐ Plants

Methods

n/a	Involved in the study
☒	☐ ChIP-seq
☐	☒ Flow cytometry
☐	☒ MRI-based neuroimaging

Antibodies

Antibodies used	For IHC: CD8 (Ventana, SP57 clone, prediluted), CD3 (Ventana, 2GV6 clone, prediluted). For in vitro stimulation and intracellular cell staining: CD107A–APC (clone H4A3, Biolegend, 1:200), CD3-BV711 (clone UCHT1, BD Biosciences, 1:40), CD4-BUV395 (clone RPA-T4, BD Biosciences, 1:100), CD8-BUV805 (clone RPA-T8, BD Biosciences, 1:20), CD69-BV421 (clone FN50, BD Biosciences, 1:20), CD137-BV605 (clone 4B4-1, Biolegend, 1:20), PD-1-PE (clone EH12.1, BD Biosciences, 1:5), IFNγ-BV786 (clone 4S.B3, BD Biosciences, 1:20), IL-2-FITC (clone MQ1-17H12, BD Biosciences, 1:20), Ki67-AF700 (clone B56, BD Biosciences, 1:20), GranzymeA-PerCP/Cy5.5 (clone CB9, Biolegend, 1:20), Perforin-PE/Dazzle594 (clone dG9, Biolegend, 1:20), and TNF-α-PE/Cy7 (clone MAb11, BD Biosciences, 1:20). For T cell enrichment after nuclei isolation for single nuclei RNA-sequencing: Alexa Fluor® 488 anti-NFATc1 antibody (Biolegend 649604, clone 7A6, 5 ul of stock 0.5 mg/mL per 1 ml of Wash and Resuspension Buffer).
Validation	All antibodies were commercially purchased and validated by the company. Validation certificates are available on company websites.

Eukaryotic cell lines

Policy information about cell lines and Sex and Gender in Research

Cell line source(s)	
Authentication	
Mycoplasma contamination	
Commonly misidentified lines (See ICLAC register)	

Palaeontology and Archaeology

Specimen provenance	
Specimen deposition	
Dating methods	

☐ Tick this box to confirm that the raw and calibrated dates are available in the paper or in Supplementary Information.

Ethics oversight	

Note that full information on the approval of the study protocol must also be provided in the manuscript.

Animals and other research organisms

Policy information about studies involving animals; ARRIVE guidelines recommended for reporting animal research, and Sex and Gender in Research

Laboratory animals	
Wild animals	
Reporting on sex	
Field-collected samples	
Ethics oversight	

Note that full information on the approval of the study protocol must also be provided in the manuscript.

Clinical data

Policy information about clinical studies

All manuscripts should comply with the ICMJE guidelines for publication of clinical research and a completed CONSORT checklist must be included with all submissions.

Clinical trial registration	NCT04015700
Study protocol	The study protocol is included as a Supplementary Information file.
Data collection	The trial was offered to all patients being evaluated for GBM at Washington University School of Medicine and patients were sequentially enrolled between July 21, 2020 and December 1, 2021. Data collection continued through July 2024.
Outcomes	The primary endpoint of the study was to determine the safety and feasibility of GNOS-PV01. All 9 patients in the study received vaccine and were eligible for safety and feasibility assessments. Safety was assessed by reported adverse events and feasibility was determined by ability and time to manufacture each patient's vaccine. The secondary endpoint of the study was 6-month progression-free survival and 12-month overall survival, both of which were assessed in all 9 patients.

Dual use research of concern

Policy information about dual use research of concern

Hazards

Could the accidental, deliberate or reckless misuse of agents or technologies generated in the work, or the application of information presented in the manuscript, pose a threat to:

No	Yes	
X	☐	Public health
X	☐	National security
X	☐	Crops and/or livestock
X	☐	Ecosystems
X	☐	Any other significant area

Experiments of concern

Does the work involve any of these experiments of concern:

No	Yes	
X	☐	Demonstrate how to render a vaccine ineffective
X	☐	Confer resistance to therapeutically useful antibiotics or antiviral agents
X	☐	Enhance the virulence of a pathogen or render a nonpathogen virulent
X	☐	Increase transmissibility of a pathogen
X	☐	Alter the host range of a pathogen
X	☐	Enable evasion of diagnostic/detection modalities
X	☐	Enable the weaponization of a biological agent or toxin
X	☐	Any other potentially harmful combination of experiments and agents

Plants

Seed stocks

Novel plant genotypes

Authentication

ChIP-seq

Data deposition

☐ Confirm that both raw and final processed data have been deposited in a public database such as GEO.

☐ Confirm that you have deposited or provided access to graph files (e.g. BED files) for the called peaks.

Data access links
May remain private before publication.

Files in database submission

Genome browser session
(e.g. UCSC)

Methodology

Replicates

Sequencing depth

Antibodies

Peak calling parameters

Data quality

Software

Flow Cytometry

Plots

Confirm that:

☒ The axis labels state the marker and fluorochrome used (e.g. CD4-FITC).

☒ The axis scales are clearly visible. Include numbers along axes only for bottom left plot of group (a 'group' is an analysis of identical markers).

☒ All plots are contour plots with outliers or pseudocolor plots.

☒ A numerical value for number of cells or percentage (with statistics) is provided.

Methodology

Sample preparation	IVS and ICS flow cytometry: The patient's PBMCs (2x5x10^5 cells) were cultured in growth media (RPMI 10%-FBS), supplemented with a cocktail of IL-2 (20 IU/mL), IL-4 (10 ng/mL), and IL-7 (10 ng/mL) cytokines, and enriched for neoantigen specific T cells using 10 ug/mL of epitope stimuli. Three days later, cells were washed and supplemented with growth media was replaced. On day 4, epitope stimuli (10 ug/mL) or controls were added and incubated for 1 hour. Cells were then fluorescently labeled with surface markers listed above followed by overnight fixation and permeabilization and then intracellulary stained with the antibodies listed above. snRNA-seq T cell enrichment flow sorting: Nuclei were isolated from frozen tumor sections (25 - 50 mg in size) from patient 2 (pre-GNOS-PV01 region 3 and post-GNOS-PV01 tumor resection) and patient 9 (pre-GNOS-PV01 region 2 and post-GNOS-PV01 tumor resection) following the 10x Chromium Nuclei Isolation Kit Sample Prep User Guide (CG000505 Rev A). To enrich for T cells, nuclei were stained with 5 ul of anti-NFATc1 antibody (listed above) per 1 ml of Wash and Resuspension Buffer for 30 min in the dark at 4 degrees C. To minimize sample loss, we did not perform a wash after incubation.
Instrument	IVS and ICS: LSRFortessa (BD Biosciences) with FACSDiva software v 8.0.01. snRNAseq: BigFoot cell sorted (ThermoFisher) with Sasquatch 1.19.13 software.
Software	FlowJo v1.0.4.
Cell population abundance	IVS and ICS: Sufficient/pure PBMCs were successfully isolated and confirmed by expected relative cell type abundance. snRNAseq: T cell enrichment was confirmed via positive control normal thymus sample.
Gating strategy	IVS and ICS: Cells were gated on PBMCs (forward scatter FSC-A vs side scatter SSC-A), singlets (FSC-A vs FSC-H), live cells (FSC-A vs Live/Dead), lymphocytes (CD3+ vs dump markers), CD8 or CD4 (CD8 vs CD4), and marker- or cytokine-positive populations were quantified within each subset. Boolean gating was performed to define combinatorial expression patterns where indicated. This gating strategy applies to all flow cytometry analysis studies presented in the manuscript.

☒ Tick this box to confirm that a figure exemplifying the gating strategy is provided in the Supplementary Information.

Magnetic resonance imaging

Experimental design

Design type	
Design specifications	
Behavioral performance measures	
Imaging type(s)	
Field strength	
Sequence & imaging parameters	
Area of acquisition	

Diffusion MRI ☐ Used ☐ Not used

Preprocessing

Preprocessing software	
Normalization	
Normalization template	
Noise and artifact removal	
Volume censoring	

Statistical modeling & inference

Model type and settings	
Effect(s) tested	

Specify type of analysis: ☐ Whole brain ☐ ROI-based ☐ Both

Statistic type for inference

(See Eklund et al. 2016)

Correction

Models & analysis

n/a	Involved in the study
☐	☐ Functional and/or effective connectivity
☐	☐ Graph analysis
☐	☐ Multivariate modeling or predictive analysis

Functional and/or effective connectivity

Graph analysis

Multivariate modeling and predictive analysis